5-2015

Effect of crimping, multilayering, and twisting on polymer fibers for ACL replacement

Mariana Ocampo
University of Texas-Pan American

EFFECT OF CRIMPING, MULTILAYERING, AND TWISTING ON POLYMER FIBERS FOR ACL REPLACEMENT

A Thesis

by

MARIANA OCAMPO

Submitted to the Graduate School of
The University of Texas-Pan American
In partial fulfillment of the requirements for the degree of

MASTER OF SCIENCE

MAY 2015

Major Subject: Chemistry

EFFECT OF CRIMPING, MULTILAYERING, AND TWISTING ON POLYMER FIBERS FOR ACL REPLACEMENT

A Thesis
by
MARIANA OCAMPO

COMMITTEE MEMBERS

Dr. Javier Macossay-Torres
Chair of Committee

Dr. Hassan Ahmad
Committee Member

Dr. Evangelia Kotsikorou
Committee Member

Dr. John Villarreal
Committee Member

May 2015

ABSTRACT

Ocampo, Mariana., Effect of crimping, multilayering, and twisting on polymer fibers for ACL replacement. Master of Science (MS), May, 2015, 95 pp., 22 tables, 52 figures, 61 references, 37 titles.

The Anterior Cruciate Ligament (ACL) is the most common knee injury in the United States; roughly 150,000 ACL surgeries are performed annually. The ACL lacks self-healing properties due to its location inside the knee's intra – articular environment (IA). Treatments for ACL ruptures involve the use of autogenous grafts or allografts. More suitable treatments can be found in new bio engineered tissue scaffolds, composed of natural and synthetic polymers. The polymers provide stronger mechanical properties and the ability to promote cell adhesion. It is believed that mimicking the crimping pattern of human ligaments will enhance polymer properties.

Four polymers were selected; Polycaprolactone and Polydioxane as natural polymers, and Tecoflex and Carbothane as synthetic polymers. All polymers were electrospun to produce nanofiber sized polymer mats. SEM images confirm smooth and oriented nanofibers for all polymer samples. Tensile strength data for uncrimped, crimped, twisted and multilayered samples confirm changes in the mechanical properties.

DEDICATION

First of all I dedicate this thesis to God almighty who has filled me with his infinite grace, wisdom and strength to be able to complete this feat and all others to come. I am eternally grateful to you my Lord. Especialmente esta thesis esta dedicada a mi madre, Patricia Vera, y a mi abuelita, Minerva Vera Fonseca, gracias por todos los sacrificios y por enseñarme todo lo que se hoy. A mi abuelita, se que desde arriba me estas viendo escribir estas palabras. Siempre estaras en mi corazon. Para ti, mamà gracias por siempre luchar por nosotros, para que obtuvieramos la mejor educacion posible y por ensenarnos que la sabiduria es mas importante que aun el dinero o el poder. Te amo mamà. I also dedicate this thesis to my brother, Octavio Ocampo, and to my sister, Victoria Ocampo. You guys are the only reason I fight for in this world. I can only hope that my achievements in my career have set a good example for you guys and to remind you to never give up no matter how dark it seems. All of our struggles will be worth it the end. Everything is hard in this life, but it will be your amount of hard work, tenacity, courage, will and dedication, that will determine how far you will succeed. To my amazing boyfriend Marcos Acosta, the amount of love and support I receive from you is entirely unbelievable. I am very blessed to be able to call you mine. Thank you for believing in me, even when I didn't believe in myself.

ACKNOWLEDGMENTS

I would like to thank my advisor, Dr. Javier- Macossay Torres, thank you for giving me the opportunity to work under you and to keep advancing in my chemistry career. Thank you for your patience with me and for all the advice and encouragement, I would not understand half the things written in here if it were not for you. To all of my committee members, Dr. Ahmad, Dr. Kotsikurou and Dr. Villarreal, thank you for being part of my team. I would also like to thank Dr. Ibrahim, Dr.Smith, and Mrs. Diaz who have been there for me since day one of my graduate school journey. All of my gratitude, for Mr. Thomas Eubanks, who helped me enormously in fixing all of my technical difficulties and for teaching me all my instrument savviness. To my dear friend and fellow colleague, Miss. Vanessa Garcia, you have been my lighthouse not only in my master thesis voyage but also in many other aspects as well. Thank you for being a great friend. Last, but certainly not least, to my favorite lab partners in the world, Monica Contreras and Daniel Martinez. You guys always made me laugh even when I didn't feel like it, thank you guys for all the love and understanding. My final thanks to the University of Texas Pan American and to the entire Chemistry Department for shaping me into the strong, educated woman I am today.

TABLE OF CONTENTS

Page

LIST OF TABLES

Page

LIST OF FIGURES

CHAPTER I

INTRODUCTION

Anterior Cruciate Ligament

Anterior cruciate ligament (ACL) ruptures are the most common knee injury amongst Americans, with an estimated 200,000 reconstructive surgeries performed annually.[1] The ACL has no ability to repair itself due to its unique location inside the knees intra - articular environment. Inside the intra - articular environment, the ACL is enveloped by synovium–containing fluid designed to lubricate the joint and prevent clots.[1] The ACL is naturally nourished by the synovium fluid and by a vascular network that goes from femur to tibia and provides long term nourishment to the ligaments.[2] However, following ACL surgery this vascular network becomes compromised and the ACL becomes entirely dependent on synovial fluid for sustenance, and because synovium fluid alone cannot provide 100% of the nutrition required, there is tissue death and changes in the ACL's mechanical properties. The current primary treatment for ACL injuries is invasive surgery requiring an autogenous graft or an allograft. Autogenous grafts are usually taken from the patient's own patellar tendon, hamstrings or quadriceps tendon. Allografts are taken from a previously deceased human donor from the same areas. Clinical studies show good to excellent results in 70-90% of autogenous grafts and similar results for allografts.[3] The drawbacks for autogenous grafts are numerous, including

additional surgery, donor site morbidity, pain when kneeling, increased recovery time, patellar irritability, quadriceps weakness and lack of graft fixation.[3] Allografts are sometimes preferred since they involve one less procedure done to the already injured patients; however, their most dangerous drawbacks lie in the risk of transmitting disease or bacterial infections, altered mechanical properties after sterilizations, and unfavorable immunogenic responses from the host.[4]

In a study conducted by Feagin and Curl, they stated that primary surgical repair alone was not sufficient to treat the ACL deficient knee and recommended the use of augmentation.[5] A variety of synthetic ligament replacements have been used, but not with much definitive success; of 855 synthetic replacements that were tracked for 15 years, about 40 to 78% of them failed due to wear debris, tissue reactions, and mechanical limitations.[1]The three most successful synthetic ligament replacements have been the polytetrafluoroethylene Gore-Tex® prosthesis, the polyester Stryker Dacron ligament, and the polypropylene based Kennedy Ligament Augmentation Device (LAD).[1]

Ligament Anatomy

Ligaments are dense, highly ordered tissues composed of proteins that are arranged in a hierarchical structure and organized into different arrangements. Ligaments are arranged in order starting with collagen molecules, fibrils, fibril bundles, and fascicles that run along the axis of the tissue.[4] The human ACL measures 38mm in length and 100 mm in width, approximately as it crosses the knee joint from the femur to the tibia in the lateral to medial and posterior to anterior directions.[6] It has been found that human ACL's contain multiple 20μm-wide collagen fiber bundles separated by columns of cells in fibrous capsules, the bundles are grouped into fascicles

that vary in size from 20 to 400μm in diameter.[7] The collagen fascicles are organized in a subsequent crimped pattern that reoccurs every 45 – 50 μm.[8] As can be seen in figure 1.1, the fibers demonstrate a periodic wave or crimp along their length, reoccurring at exactly that range, and in some cases bundles of fibers form distinct fascicles, which may serve a functional role in the distribution of forces.[9]

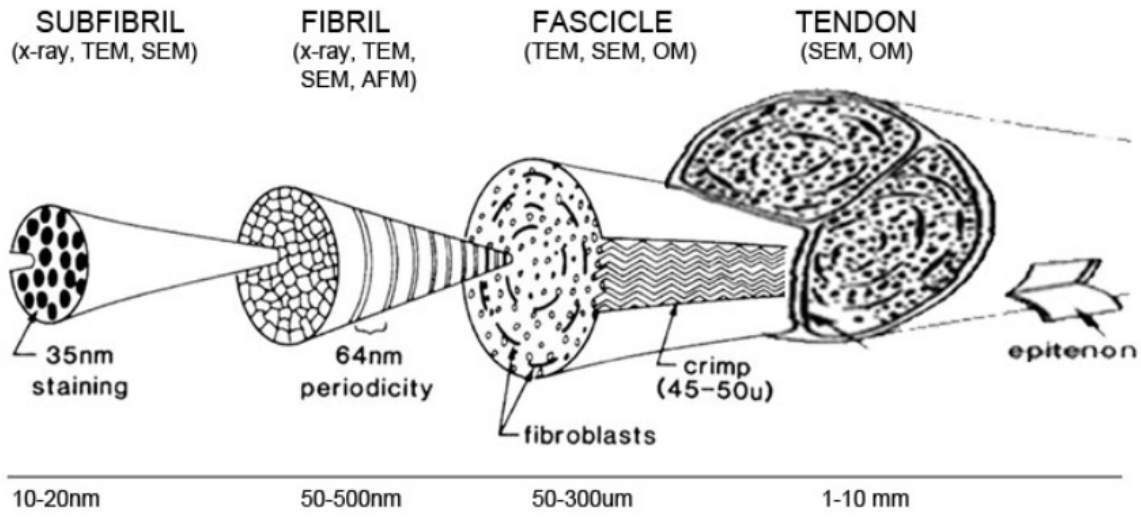

Figure 1.1: Organization of Ligaments and Tendons [10]

Ligaments are primarily composed of water 60 to 70% and of a highly ordered structure of collagen. Collagen makes up about 75% of the dry weight of the ligament, the majority of the collagen (90%) is type I, with type II making up the remaining (10%).[7] Elastin, present in small amounts (<5%) [7], is responsible for providing some of the tensile resistance and elastic recovery exhibited by the ligaments due to its interactions with the collagen fibers. Proteoglycans have an important role in organizing the Extracellular Matrix (ECM) and interacting with tissue fluids, they make up only about 1% of the ACL dry weight.[7] Glycoproteins such as fibronectin or lamimin are also present in the ACL and are thought to facilitate interactions between cells and their surrounding matrix.[7]

The crimping pattern exhibited by the collagen fibers has been proven to be a universal phenomenon and is exhibited in tendons of all animals as well as in numerous other collagenous tissues which are subjected to tensile loading in their respective organisms.[11] Even though the crimping effect is universal, the mechanical properties are subject to change systematically with development and age, as the age increases the wavelength increases and wave crimping angle decreases.[11] On average, the ACL withstands cyclic loads of 300N around 1-2 million times per year. For example, when ascending a set of stairs, the ACL experiences 67N of tensile force. When jogging, it experiences 630N of tensile force.[12] As aging occurs, accompanied by weight changes, wear and tear of the ACL becomes significantly pronounced. For example, the force required to rupture the ACL decreases by almost 60% between the ages of 20 and 60.[9] Figure 1.2, illustrates the stress-strain relationship of fibers, when the crimped fibers are under stress, they first exhibit an area of very low stress, known as the "toe region". In the "toe region", the crimped collagen fibers begin to straighten out and the force begins to be directly translated to the fibers. This second region is known as the "linear region", and is characterized by a sharp increase in its slope. In the linear region, all the individual fibers are uncrimped and are enlisted in helping with the stress load. The increase in stress load leads to the collagen triple helix becoming fully stretched and interfibrillar slippage begins to occur between the cross links, leading to failure of the fibers.[4] The last region known as the "yield or failure region", is characterized by a sharp decrease in slope and signifies that the collagen fibers have become ruptured, rendering the fibers unable to bear any stress.

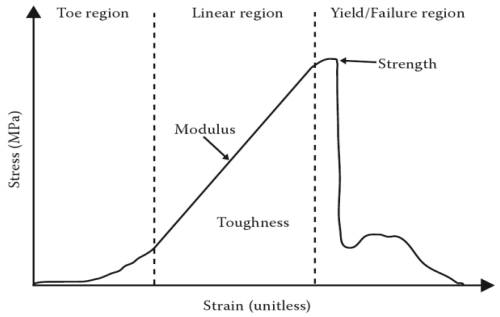

Figure 1.2: Stress – Strain Relationship of Ligaments [13]

It should be noted that the existence of a crimp pattern in ligaments is what gives the ligaments the ability to partially recruit some of the fibers when experiencing low everyday stress forces. Due to their crimped nature, crimped fibers are believed to have an advantage that should render them able to withstand larger tensile stress loads and increases their extension.[4]

Bio - Engineered Tissue Scaffolds

Current surgical and synthetic methods for treatment of ACL ruptures are not suitable long term solutions. While they do provide some benefits, the disadvantages are sometimes too costly for the patients. A new ACL replacement which retains the strength of the original ACL, while remaining safe and painless to the patient, is required. This need has led research to focus on the development of Bio - engineered tissue scaffolds. Tissue engineering can be defined as the application of biological, chemical and engineering principles toward the repair or restoration of living tissues using biomaterials, cells and other factors alone or in combination.[14] Biodegradable scaffolds that can provide a temporary template for structural and logistic tissue development, will be the main focus of this research. Some of the key requirements for an ideal scaffold include a fibrous matrix customized for ligament tissue engineering, wire rope structure,

mechanical properties matching those of native ligaments, high porosity to allow cell infiltration and biodegradation at a rate matching that of tissue formation.[1]Scaffold structure and scaffold material are important in facilitating the transport of nutrients, metabolites and regulation molecules to and from the seeded cells. Scaffold structure and material will also determine the mechanical properties and the ability of the scaffold to mechanotransduce at the cellular and tissue levels. [1] The current standards that would make an adequate ACL graft are set at 1730 N for tensile strength, 182 N/mm for linear stiffness, and 12.8 N-m for energy absorbed at failure.[15] The scaffold material must also be biocompatible and must biodegrade at a rate matching the rate of new tissue formation. Two of the most promising biomaterials for scaffolds have been collagen and silk fibers. Collagen supports cell attachment, spreading, and fiber coverage with extracellular matrix deposition. However, poor mechanical integrity of the fibers and the risk of leached chemical cross linking agents determine collagen is not the best biomaterial. Silk fibers have also shown promise since they are cheap to make, are biocompatible, degrade at a good rate, support spreading and attachment of cells and have customizable mechanical properties. Some silk fibers have shown mechanical properties similar to those of a functioning ACL when woven into the appropriate wire rope geometry.[16] Accelerated tissue degradation along with failure to provide adequate mechanical performance in a demanding mechanical environment over a sufficient time frame to allow for new tissue formation makes all current scaffold materials inadequate.[16] It is of extreme importance that potential scaffolds incorporate all of the ACL's mechanical properties into the matrix design; linear stiffness and ultimate tensile strength (UTS) must be maximized if host tissue ingrowth and constant biological remodeling are to be the primary means of knee joint stabilization over the long term.[16] Synthetic polymers have also

been tested as potential material for the scaffolds, while both synthetic and natural biomaterials offer some good biological characteristics, they still need to be further developed.

Tissue engineered scaffolds must be fabricated with the right sized fibers in order to mimic the human ECM as closely as possible. Within the past decade, the potential of nanofiber producing systems has been developed and explored to create suitable scaffolds for tissue engineering. Nanofibers have the potential to provide enhanced cell adhesion due to the similarity of their 3D architecture to the human ECM. The high surface area to volume ratio of the nanofibers combined with their microporous structure favors cell adhesion, proliferation, migration, differentiation and provides an excellent environment for cells to grow and perform.[17] Nanofibers are typically produced through electrospinning, self-assembly or phase separation. The electrospinning process can produce fibers ranging from 50 to about 1000 nanometers (nm) or greater; nanofiber alignment can also be achieved through electrospinning.[17] It has been recognized that smaller fiber diameters provide high surface areas and enhanced mechanical properties.[18] In a study conducted by Vasita and Katti, it was concluded that aligned nanofibrous scaffolds showed promise for use in ligament tissue engineering.[17]

History of Electrospinning

The phenomenon of electrostatic attraction was first observed in the 1500's by Sir William Gilbert. He first observed that an electrically charged piece of amber formed a cone shape near a droplet of water and smaller droplets were ejected from the tip of this cone.[19] In more modern times, the phenomena was once again observed by Rayleigh in 1897 and in 1900 John Francis Cooley was granted the first electrospinning patent. The first attempts at trying to mathematically model the behavior of fluids under electrostatic forces was undertaken by John

Zeleny in 1914, with his published work on the behavior of fluid droplets at the end of metal capillaries.[20] In 1934, Anton Formhals was granted the first US patent for a commercial electrospinning setup for the production of textile yarns. Cellulose acetate was electrospun using acetone and monomethyl ether of ethylene glycol with a voltage of 57 kV.[21] In 1964, Sir Geoffrey Ingram Taylor published his last research paper titled "Disintegration of water drops in an electric field".[22] His mathematical research laid the groundwork for understanding the electrostatic forces responsible for the electrostatic phenomena. When an electrical charge is applied, the Coulombic repulsion forces between charges of the same polarity produced in the polymer liquid by the emitting electrode destabilizes the hemispherical droplet of the polymer liquid at the tip of the nozzle to finally form a droplet of conical shape.[23] This cone formation is now commonly known as the Taylor cone, as the applied electrostatic field strength increases the Coulombic repulsion force, it exceeds that of the surface tension which results in the ejection of an electrically charged jet of polymer liquid. The charged jet travels in a straight path for small distances before it undergoes a bending instability and forms a looping path. During its path to the collector, the charged jet elongates while drying out or solidifying, depositing ultrafine fibers on the collector.[23] The term electrospinning did not become popular until the 1990's when Reneker's research group coined the term; since 1995 the electrospinning process has been increasingly revisited due to increased interest in nanofibers and their potential uses. Over 200 universities worldwide are engaged in electrospinning and electrospun fiber applications.[21] The fibers produced by electrospinning can be manipulated in a variety of different ways and their final diameter size, alignment and structure all depend on the parameters applied during the electrospinning process.

Electrospinning Parameters

In terms of versatility, flexibility and ease of fiber production, there is no other process that can match the elctrospinning setup. At its most basic form, it simply requires high voltage power suppliers, a syringe, a needle and a charged collector. Figure 1.3, is a simple schematic of an electrospinning apparatus with its basic components and a rotating collector, such as the one we use in this research.

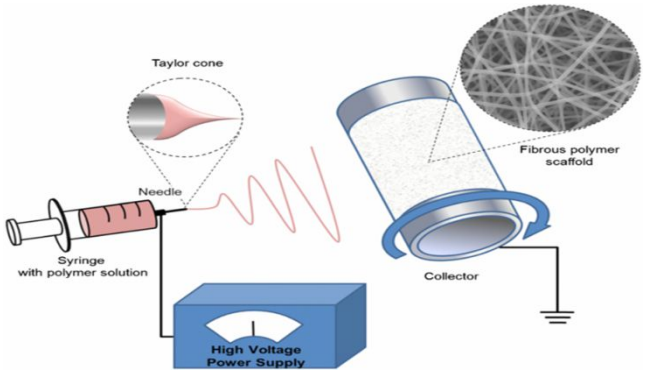

Figure 1.3: Electrospinning Setup [24]

Electrospinning can produce nanofibers from a variety of materials, including polymers, composites, semiconductors and ceramics.[25] However, this research will focus solely on the production and characterization of nanofibers produced from soluble polymers. The electrospinning process is controlled by two sets of parameters: system parameters and process parameters. Each electrospinning setup is different, so the system and process parameters for each case lend themselves to modification, facilitating the tailoring of electrospun nanofibers with unique mechanical characteristics. Certain mechanical properties are affected by the properties of the polymer, and other mechanical properties are affected by how the polymer has been electrospun. System parameters such as polymer molecular weight and polymer distribution determine the rate of degradation of the nanofibers. System parameters also involve inherent

polymer solution properties ; viscosity, surface tension, and conductivity all determine the nanofiber diameter and reduce the possibility of bead formation.[17] Process parameters such as needle tip diameter, flow rate of polymer and electric potential also play a role fiber diameter. Distance between the needle tip and collector determine the extent of solvent evaporation from the nanofibers and deposition on the collector; collector motion also determines the pattern formed during fiber deposition.[17] Several studies have shown that reducing solution concentration will reduce the diameter of the electrospun fibers, and reducing needle tip to collector distance will increase inter-connectivity of the fibers.[25] Increasing rotational speed of the collector will also increase fiber alignment ; in a study done by Matthews et al,[26] it was shown that at speeds of less than 500 rpm, a random mix of collagen fibers was obtained, when the rotational speed was increased to 4500 rpm, the collagen fibers showed a significant increase in alignment.[26] Nanofiber alignment is important since it allows the cells to proliferate in the direction of the alignment, in tissue engineering applications this directional neuronal/axonal growth is desired.[17] Mechanical properties such as Young's modulus, yield stress, and tensile stress have also increased with higher rotational speed and fiber alignment.[25]

Bio and Synthetic Polymers

Biopolymers are polymers that can be biodegradable, bioresorbable, bioabsorbable and bioerodable.[27] Synthetic polymers are derived from petroleum based components and can be produced artificially. For ligament replacement applications, bioresorbable polymers are ideal because they are eliminated from the body completely, including starting foreign materials, bulk degradation products, and by-products with no side effects. Biopolymers are natural polymers

that can be found in nature, in our own bodies, and can be synthesized from natural biological materials. In the human body for example, our DNA and RNA contain polymer backbones, the starch and cellulose we require to perform our daily activities are also natural polymers. Most of our muscles, ligaments and tendons are composed of proteins and collagen which are natural polymers. Synthetic polymers provide the basis for the production of plastic bags, rubber tires, clothing, electronics, as well as many other conveniences. Nylon, Teflon ^{TM}, polyester, and polyethylene are just a few of the synthetic polymers available. Most synthetic polymers are able to provide a strength and durability that natural polymers cannot yet they lack biocompatible features .For this research we choose two biopolymers and two synthetic polymers: Polycaprolactone and Polydioxanone as the former, and Tecoflex ™ EG 80A and Carbothane™ 3575A as the latter. The rationale for these selections will be elaborated upon below.

Polycaprolactone

Polycaprolactone (PCL) was one of the earliest polymers to be synthesized in the early 1930's. PCL can be prepared by either ring-opening polymerization of Ɛ-caprolactone using a variety of anionic, cationic, coordination catalysts, and via free radical ring-opening polymerization of 2-methylene-1-3-dioxepane.[27] PCL is a semi-crystalline, hydrophobic polymer; it is usually sold in clear/white pellets or granules. PCL has many desirable characteristics such as good solubility, low melting point, excellent blend compatibility and an average degradation rate of 2-4 years.[27] The human body does not possess the enzymes required to biodegrade PCL. However, PCL is bioresorbable via slow hydrolytic degradation. In the first stage of the degradation process, there is non-enzymatic hydrolytic bond cleavage of the ester groups. In the second stage, when the polymers crystallinity has increased and its molecular

weight has dropped to less than 3,000 g/mol, the polymer undergoes intracellular degradation.[27] The cleaving of the ester groups, allows the remaining fragments to recrystallize into small , highly ordered groups with an overall lower molecular weight and higher crystallinity. Observations of PCL fragments in phagosomes, giant cells, and inside fibroblasts, support the theory that PCL is completely resorbed, degraded and excreted from the body once the molecular weight drops.[27] Figure 1.4 shows the mechanism and excretion cycle of PCL from the human body.

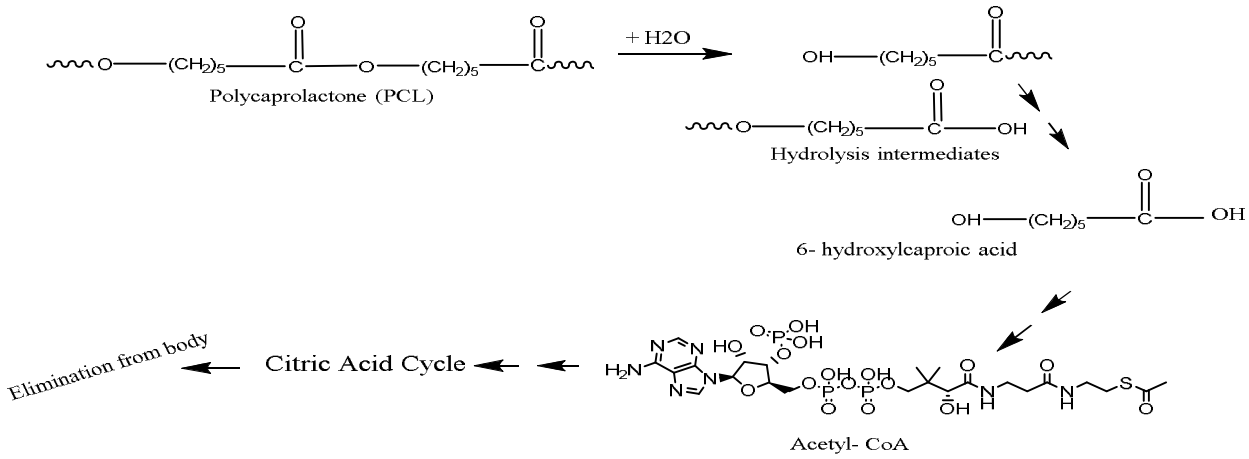

Figure 1.4: Degradation of Polycaprolactone [27]

The sole metabolite in the PCL degradation mechanism is 6-hydroxyl caproic acid. Hydrolysis intermediates of 6-hydroxyl caproic acid and of acetyl coenzyme A are formed enter the citric acid cycle and are eliminated from the body.[27] In the medical field, PCL has limited applications, acting as drug delivery devices, wound dressings or as biocompatible sutures. PCL is an almost perfect biopolymer for use inside the human body; however, the weak mechanical properties of PCL make it unsuitable for high load bearing applications. That does not mean PCL has been cast off, recently there has been renewed interest in PCL due to the growing field of tissue engineering. The biocompatibility, slow degradation time and unique rheological properties of

PCL have made it the biopolymer of choice for many of the ongoing tissue engineered scaffold studies.

Polydioxanone

Polydioxanone (PDO) is a colorless, crystalline, bioabsorbable polymer; it was specifically developed in the 1980s as the first monofilament wound closure sutures.[28] PDO exhibits high flexibility, higher strength retention and lower inflammatory responses than that of PGLA or PGA.[28] The extra flexibility of the PDO polymer is due to the incorporation of an ether oxygen group present in the backbone of the structure. PDO has a moderate reabsorption rate of months instead of years and low surface friction that allows it to glide smoothly through tissues. PDO retains shape memory and will always want to coil back to its original shape. This low surface friction combined with its memory shape retention makes PDO knot retention extremely difficult.[28] PDO is formed via ring opening polymerization of paradioxanone with heat and an organometallic catalyst such as diethylzinc or zinc l-lactate, figure 1.5. The reaction results in the formation of PDO which is now a poly (ether-ester), PDO degrades through the non-specific scission of the ester back bone. PDO is a highly crystalline and hydrophobic polymer, which enables its degradation rate to be slow to moderate. In the human body, PDO is broken down into glycoxylate and is excreted, figure 1.6, in human urine or converted into glycine, then into carbon dioxide and water.[29]

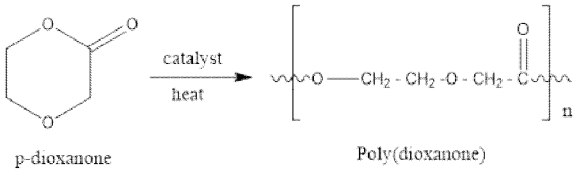

Figure 1.5: PDO polymerization reaction [28]

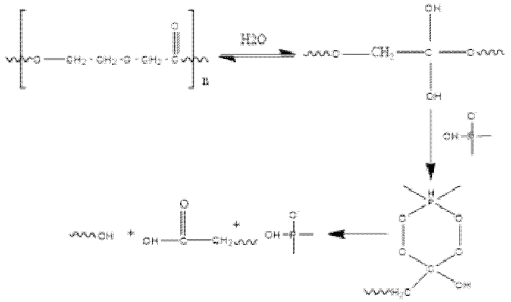

Figure 1.6: Hydrolysis of aliphatic polyesters such as PDO in phosphate buffer [30]

PDO is mainly utilized as sutures but it has also been applied in orthopedics, plastic surgery, drug delivery, cardiovascular repair and bone repair applications.[28] Expansion of PDO in the medical field has been slowed down due to the mixed results obtained from these various applications. PDO has limited used in the medical field, but in the growing field of tissue engineering, PDO is a very promising polymer for potential use in tissue engineered scaffolds. Its biocompatibility, flexibility, degradation rate, shape retention and low inflammatory response make it suitable for future tissue engineering applications.[28]

Tecoflex™ EG 80A

Tecoflex™ EG 80A belongs to a class of aliphatic polyether based thermoplastic polyurethanes (TPU's). Polyurethanes are composed of three different components; a polyol (P), a diisocyanate (D) and a chain extender (C). The polyol, or soft segment, is an oligomeric macromonomer compromising a chain with a low glass transition temperature and terminated by hydroxyl groups. The chain extender is usually a small molecule with either hydroxyl or amine end groups. The diisocyanate is a low molecular compound that can react with the polyol or the chain extender; the combination of the chain extender and the diisocyanate make up the hard segment of the polymer.[31] Most polyethers have a repeating structure of –R-O-R- with chain ends of hydroxyl groups.

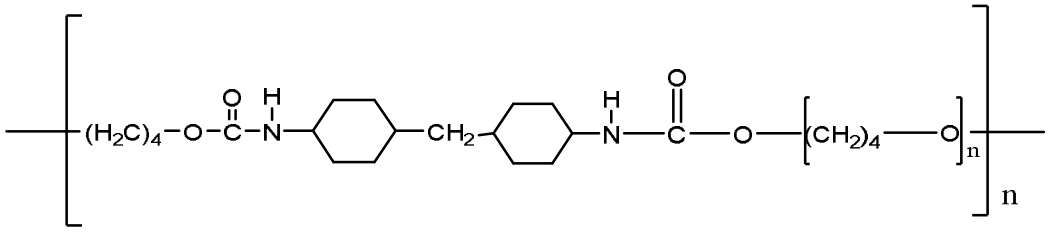

Figure 1.7: Structure of Tecoflex™ EG 80A [32]

Thermoplastic polyurethanes have many useful properties including elasticity, transparency, oil, grease, and abrasion resistance. In the 1950's Lubrizol developed the first commercial TPU's. Since then, TPU's have been used in the medical field for their strong mechanical properties, good blood compatibility and biodegradation. TPU's differ from earlier polyurethane materials since they form linear, non-crystalline polymers that can be melted at reasonable temperatures. TPU's are also soluble in a variety of solvents and can be melted and reformed using conventional or extrusion equipment. Studies have shown that some polyether-urethane polymers are susceptible to crack formation and propagation when the stress level on the polymer is high. Polyether-urethanes undergo hydrolytic degradation, but certain materials can be employed when degradation is not wanted, such as aromatic diisocyanates. However, aromatic diisocyanates have harmful carcinogenic effects. Degradable polyurethanes are commonly made from diisocyanates such as lysine-diisocyanate (LDI), hexamethylene diisocyanate and 1, 4 diisocyanate whose degradation products are more likely to be non-toxic, i.e.lysine.[31] Currently, there are studies being done to establish the exact degradation and functionality of Tecoflex for future use as a material for tissue engineered scaffolds.

Carbothane™ 3575A

Carbothane belongs to a class of aliphatic and aromatic polycarbonate based thermoplastic urethanes (PC-TPU's). Polycarbonate TPU's are made by reaction of bisphenol A (BPA), a diphenyl carbonate and phosgene ($COCl_2$), which polymerize to produce polycarbonate. General Electric researcher, Daniel W. Fox, was the first to accidently create polycarbonate which was trademarked in the 1960's as Lexan®.[33] Polycarbonates are widely used as high-performance engineering polymers due to their excellent impact resistance. The

polycarbonate polymer is stronger, functional over larger temperature ranges, and has a higher light transmission than glass. Polycarbonates have a high glass transition temperature of about 147°C, and they can undergo large plastic deformations without breaking or cracking.[34] These properties make polycarbonates easy to work with at room temperatures and allow for them to be processed and molded using a variety of techniques. Polycarbonates are used in practically every industry, i.e. in the medical fields as tubing, bullet resistant windows in cars, air fighter jets use a polycarbonate piece as their roof , greenhouse sheets, CD's, DVD's, as well as safety lab goggles . There has been growing concern with the used of BPA due to its possible carcinogenic nature and for this reason, other diols have been tapped as replacements for BPA. BPA derived products also have a tendency to crystallize, to reduce that, other additives such as cyclohexane are used as comonomers in the production of polycarbonates. Tetrabromobisphenol A is added to increase fire resistance tetramethylcyclobutanediol and dihyroxybenzophenone have been developed as future BPA replacements.[35] Deeper understanding of how polycarbonates degrade has only recently begun to take shape. In the 1990's, research groups reported no evidence of hydrolytic degradation of polycarbonates; however, more recent studies have exposed polycarbonates to cholesterol esterase (CE) to study the degradation of PC-TPU'S.[36] Several studies conducted by Tang, [36] Finer, [37] and Suyama et al, [38] have shown that the degradation of polycarbonates is a lot slower than that of ester containing polymers. Suyama studied the degradation effect of CE on an aliphatic polycarbonate that began to exhibit sign of molecular degradation in as little as one week. It was also noted that changing the hard segment size and/or chemistry could significantly alter the bio stability of the PC-TPU's.[36, 39, 40] It is important to note that Suyama's study was conducted using an aliphatic polycarbonate, whereas Carbothane™ 3575A is alicyclic, and previous studies have shown that degradation occurs at a much slower rate. Further research still

needs to be conducted to completely understand the many variables of polycarbonate degradation. Carbothane™ 3575A is sold commercially by the Lubrizol Company; it is composed of dicyclohexylmethane-4, 4′-diisocyanate (H_{12}MDI) for the rigid segment and 1, 4-butanediol for the chain extender.

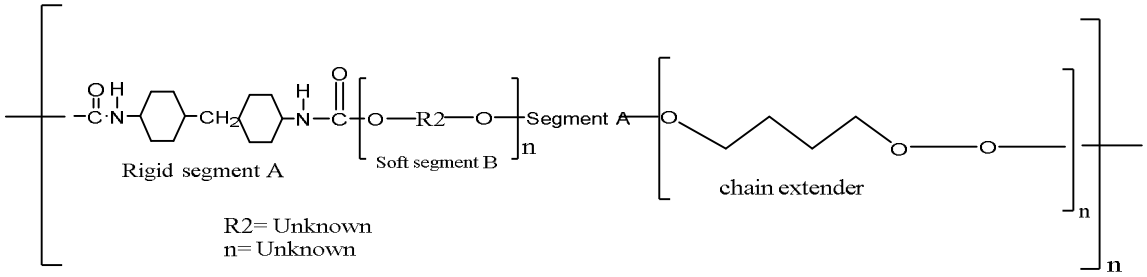

Figure 1.8: Structure of Carbothane™ 3575A [41]

The precise chemical structure of the polycarbonate soft segment are not disclosed to the public.[41] Carbothane is characterized by an excellent oxidative stability, good mechanical properties, and good chemical properties.[42]

Current Thesis Goals

It is evident that a new type of ACL replacement is needed. Current methods have proven to be only temporary and only help patients attain limited knee activity. Even though autografts are by far the most successful of all the available replacement methods, complications such as donor site morbidity, limited supply, and long-term problems have been the driving force behind implementing tissue engineering as a new technique. From a ligament tissue engineering aspect, scaffolds can jumpstart the regenerative process and eventually lead to new, fully developed, living ligaments. Both natural and resorbable synthetic polymer-based scaffolds are being developed as alternatives to current ACL replacement options. The scaffolds must meet key requirements such as biodegradability, biocompatibility, and appropriate support of knee

loads. The scaffolds must be able to replicate the stress-strain curve behaviors of the native ACL, allow for cell infiltration, and promote new tissue growth. Research continues to be done on various ways of trying to achieve a long term viable scaffold option. Different scaffolds have already been constructed with cross-linked polymers and have gone on to be seeded with cells such as fibroblast or bone marrow stromal cells.[43] The overall scaffold design is another key requirement, since the chosen design must mimic the structure of the native ACL. It has been reported that twisting and braiding tend to increase the mechanical properties of the materials [4,14,16,44], prompting further exploration of these designs. Scaffolds that were highly aligned have also shown an increase in mechanical properties as well as cell seeding in the direction of alignment.[45] Though it has not yet been achieved, research in the ligament tissue engineering field remains strong in the search for a scaffold that will help regenerate the ACL and provide it with new tissue that will match the native tissue both mechanically and biologically. The focus of this thesis was to investigate the mechanical and biological behaviors of scaffolds prepared from PCL, PDO, Tecoflex™ EG 80A and Carbothane™ 3575A. To increase the mechanical properties of the scaffolds, they were electrospun at high rotational speeds to promote high alignment. It was hypothesized that crimping the scaffolds would allow their mechanical properties to mimic those of native crimped human ACL fibrils. The crimping effect theoretically causes scaffolds to obtain a stress – strain curve closer to that of native ACL. Twisting of the scaffolds was also studied in an effort to increase mechanical properties and stability to the scaffolds. It was also hypothesized that multilayering the scaffolds with a natural gelatin would increase the viscoelastic properties of the scaffolds. The crimping pattern is implemented in each different polymer design to observe if crimped scaffolds had mechanical properties similar to those of native human ACL. The purpose in obtaining this data is to

contribute to the search for a suitable tissue replacement scaffold, which will meet all the mechanical requirements necessary to become a new ligament replacement scaffold.

CHAPTER II

MATERIALS AND METHODS

Polycaprolactone (PCL) (M_n= 70K-90K) purchased from Sigma-Aldrich, and Polydioxanone (PDO) acquired from Evonik Industries were used as the biocompatible and biodegradable polymers. The biocompatible, yet non-biodegradable polymers, Tecoflex™ EG 80A and Carbothane™ 3575A were kindly supplied by the Lubrizol Corporation. Edible beef gelatin was obtained from the PB Leiner Corporation. N, N- Dimethylformamide (DMF) 99 % from Acros Organics, deionized water (DI H_2O) from the laboratory, glacial acetic acid (AA) from Fisher Scientific, 1,1,1,3,3,3-hexafluoro-2-propanol 99% (HFIP) from Oakwood Chemical, and Tetrahydrofuran (THF) 99.8% extra dry stabilized from Acros Organics, were used without further purification.

Electrospinning

For delivery of the polymer solutions a 10 mL glass syringe from Chemglass Life Sciences along with a 22 gauge, 2 inches long, needle from The Hamilton Company were used. A KDS-200 syringe pump from KD Scientific Holliston, Inc., MA, was used to control flow rate. Two high voltage (HV) suppliers from Gamma Research (Ormond Beach, FL); a HV Power Supply Model No. ES30P-5W and a Model No. ES30N-5W were used for the positive and the negative voltages respectively. The optimized electrospinning parameters for PCL, PDO, Tecoflex™ EG 80A, Carbothane™ 3575A, and beef gelatin are presented in Table 2.1.

Polymer (W/V)	Solvent	Collector Voltage	Needle Tip Voltage	Needle to Collector Distance	Flow Rate (mL/min)	Collector RPM
PCL 10%	THF/DMF (1:1)	-20kV	+20kV	22cm	0.03 mL/min	5000 rpm
PDO 12.5%	HFIP	-20kV	+20kV	22cm	0.03 mL/min	5000 rpm
Tecoflex™ EG 80A 15%	THF/DMF (1:1)	-20kV	+20kV	12cm	0.03 mL/min	5000 rpm
Carbothane™ 3575A 15%	THF/DMF (1:1)	-20kV	+20kV	12cm	0.03 mL/min	5000 rpm
Beef gelatin (1%)	AA/ DI-H_20 (1:1)					

Table 2.1: Electrospinning Parameters

Crimping

Crimping was applied to the polymer mats, with the use of two crimped cooper metal plates, measuring 4 in long X 1.5 in wide, each containing 8 microfolds per inch. The crimped plates were then placed in between two other metal sheets and fastened by six nuts and bolts. Figure 2.1, shows the individual crimped copper sheets used to imprint the polymer samples along with the metal sheets used to apply pressure. Crimping temperatures for each polymer were chosen between 5 to 10°C below their melting point and required a specific set of parameters, which are outlined in Table 2.2.

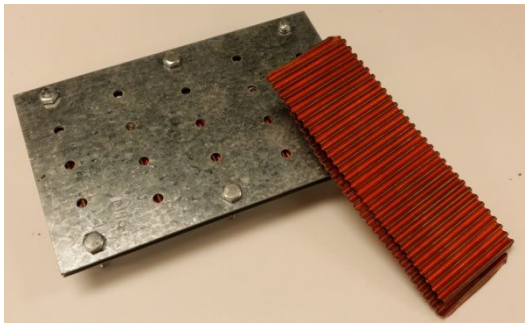

Figure 2.1: Crimping Apparatus

Polymer	Temperature (°C)	Time (Hr)
PCL	55 °C	1.5-2 hrs
PDO	85 °C	1.5-2 hrs
Tecoflex™ EG 80A	95 °C	1.5-2 hrs
Carbothane™ 3575A	35 °C	1.5-3 hrs

Table 2. 2: Crimping Parameters

Multi-layering

Multi-layering of the electrospun polymer mats was performed using beef gelatin (1% w/v), that was dissolved in 5 mL acetic acid and 5 mL DI H_2O. The polymer mats were divided into three sections and coated with a thin layer of 1 % (w/v) beef gelatin, then layered atop of each other. The polymers mats were 9.5 cm in length X 4 cm wide. They were placed in large Petri dishes lined with parafilm to prevent sticking, then placed in the oven for 30 minutes at 37°C. The samples were removed, covered with parafilm except for a small opening at an edge and placed under a vacuum desiccator to completely dry overnight.

A modified multilayering procedure was also done using beef gelatin (0.1% w/v) that was dissolved in 10 mL warm DI H_2O . The beef gelatin mixture was then poured into a parafilm lined Petri dish and the multilayered scaffolds were dip coated into the beef gelatin mixture. The coated multilayered scaffolds were allowed to drip off the excess beef gelatin and were transferred to a clean parafilm lined Petri dish. They were then placed in the oven for 30 minutes at 37°C. The samples were removed, covered with parafilm except for a small opening at an edge and placed under a vacuum desiccator to completely dry overnight.

Twisting

Twisting of the electrospun polymer mats was done using a three strand, custom made twisting apparatus. The polymer mats were cut into three equal strands and placed on individual grips that were placed 120° apart from one another. All three strands were attached to a single grip placed 8 cm from the rotor. The motor was rotated manually and the strands were twisted until they made one complete twisted strand. Figure 2.2, is a picture of the custom made three stand twisting apparatus, showcasing the 120° separation between each grip.

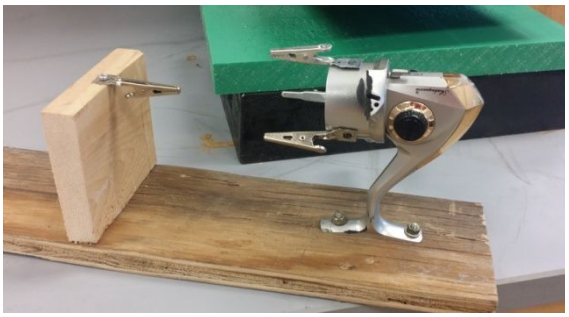

Figure 2.2: Three Strand Twisting apparatus

Scanning Electron Microscopy

Sections of the electrospun polymer mats were cut into 1 cm X 1 cm squares, placed on a specimen grid, and coated with palladium for 60 seconds at 45 mA using a Desk II Denton Vacuum Cold Sputter Coater. A ZEISS EVO LS10 Electron Microscope was then used to view the samples. The SEM micrographs were used to measure the fiber diameters using, Image-Pro Insight from Media Cybernetics. Fiber diameters were determined using the 2K magnification micrographs.

Tensile Strength Testing

Ten "dog bone" shaped specimens were cut from each electrospun polymer mat for tensile strength analysis. Test specimens were 2.75 mm wide at their narrowest point with a gage length of 7.5 mm to assure uniformity and to isolate the failure point away from the grips. Uniaxial tensile testing was performed to failure with $n \geq 8$ test specimens for every polymer mat that was electrospun, crimped, multilayered and twisted. Samples were tested on the Instron 5943 instrument with a 250 N max load cell at an extension rate of 10.0 mm/min.

Fourier Transform Infrared Spectroscopy

A small sample of the electrospun fiber mats were cut into 1 cm X 2 cm rectangles, and analyzed using a Bruker ALPHA Platinum ATR FT - IR spectrometer. The samples were analyzed using a resolution of 4 cm^{-1}, 24 scans and spectral range of 3500-400 cm^{-1}. Beef gelatin was also analyzed to be used as a reference for multilayered samples and observed peak differences

Biodegradation Testing

Scaffolds are difficult to work within joints due to the presence of enzymes in synovial fluid, which are known to degrade materials that would be stable in other parts of the body. Synovial fluid is composed of hyaluronan, D-N-acetylglucosamine, and the enzymes matrix metallopeptidase-1 (MMP-1), elastase, and plasmin in varying concentrations. In theory, these enzymes affect the healing of intra-articular injuries. MMP-1 is known to breakdown the extracellular matrix, tissue remodeling, and degrades type I, II, and III collagen. Elastase is a peptidase that breaks down elastin and collagen fibers. Plasmin is increased in the synovial fluid after an injury and known to degrade fibrin clots. [46] This current study introduced the scaffolds to

these three different enzymes, each with a concentration found within the intra - articular knee joint.

The MMP-1 stock solution was prepared by dissolving 50 mg of MMP-1 (Worthington Biochemical Corporation) in 200 mL of PBS, yielding a 250 μg/mL (72.2 units/mL) MMP-1 solution. 15 mL aliquots of the solution were frozen at −80°C in 15 cc tubes. [46]

The elastase stock solution was prepared by dissolving 5 mg of elastase (Worthington Biochemical Corporation) in 50 mL of PBS, yielding a 100 μg/mL (0.86 units/mL) solution. 15 mL aliquots of the solution were frozen at −80°C in 15 cc tubes.

Triplicates of each polymers were cut with a sterilized 6 mm biopsy puncher and placed into a 12-well plate. 1 mL of each enzyme solution was placed into the wells. Each enzyme had its own well plate. The well plates were incubated at 37°C and 5% CO2 for two weeks, changing the enzyme solution every two days. After the two week incubation period they were kept for 12 hours to dry at 35°C. Raman analysis and SEM testing was done on the scaffolds to complete the biodegradation testing.

CHAPTER III

RESULTS AND DISCUSSION

Scanning Electron Microscopy and Biodegradability

Scanning Electron Microscopy produces large magnified images using electrons instead of light. This produces images that are extremely detailed, with high resolutions and depth imaging. Inside the electron microscope, a beam of electrons is produced by an electron gun, the electron beam is directed in its path by electromagnetic fields and lenses, which focus the beam down toward the sample. Once the electron beam hits the sample, electrons and X-rays are ejected from the sample itself. Detectors inside the SEM collect the X-rays, backscattered electrons, secondary electrons and convert them into a signal that is sent to a computer screen to produce the final image. Samples that will be analyzed in an SEM must be conductive, all non-metal samples, such as polymer samples, need to be made conductive by covering the sample with a thin layer of conductive material.

Scanning electron microscopy was used to determine fiber alignment for all electrospun polymer samples. All of the micrographs obtained for the four different polymers, show continuous, uniform, and smooth bead free nanofibers that are highly aligned in the vertical direction. The micrographs obtained were used to determine fiber diameter for all polymer samples, using Image Pro software. Figure 3.1 displays the SEM micrographs of electrospun

PCL fiber mats at 150X, 400X and 2K magnification. Fiber diameter for PCL was determined to be 2.78 µm. Figure 3.2 displays the SEM micrographs of crimped PCL fiber mats at 150X, 400X and 2K magnification. PCL crimped fiber diameter was determined to be 9.65µm.

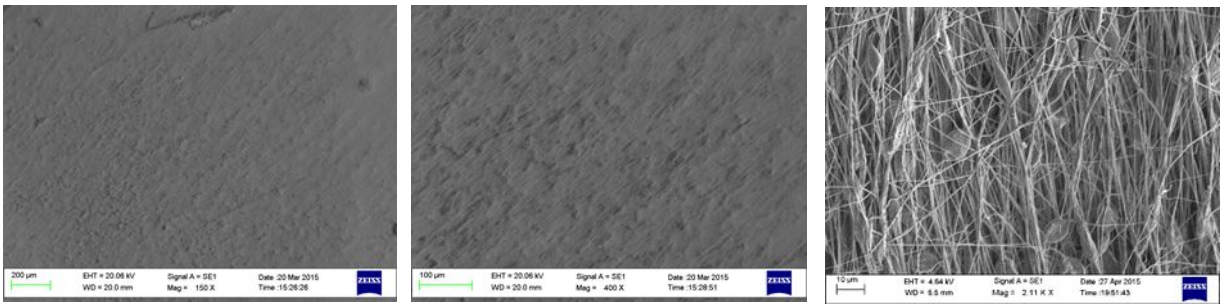

(a) (b) (c)

Figure 3.1: Scanning Electron Micrographs of PCL at (a) 150X (b) 400X and (c)

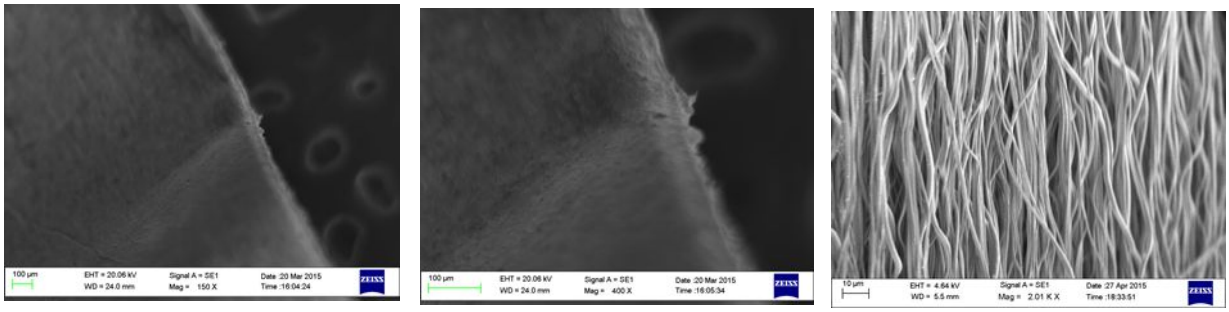

(a) (b) (c)

Figure 3.2: Scanning Electron Micrographs of crimped PCL at (a) 150X (b) 400X and (c) 2K

Figure 3.3 displays the SEM micrographs of PCL fibers after being incubated with MMP-1 at three different magnifications, 150X, 400X and 2K. The PCL – MMP-1 fiber diameter was determined to be 2.78 µm. Figure 3.4 displays the SEM micrographs of PCL fibers after being incubated with Elastase solution at three different magnifications, 150X, 400X and 2K. The fiber diameter for PCL – Elastase was determined to be 2.31µm. According to the quality of the fibers as shown in the micrographs, equal degradation of the fibers is shown. The mean of the fiber diameters for all the enzymes attest for equal degradation of the fibers by showing a

decrease when compared to the mean prior to incubation. PCL contains a carbonyl group that is able to be attacked and hydrolyzed for degradation by both enzymes.[26]

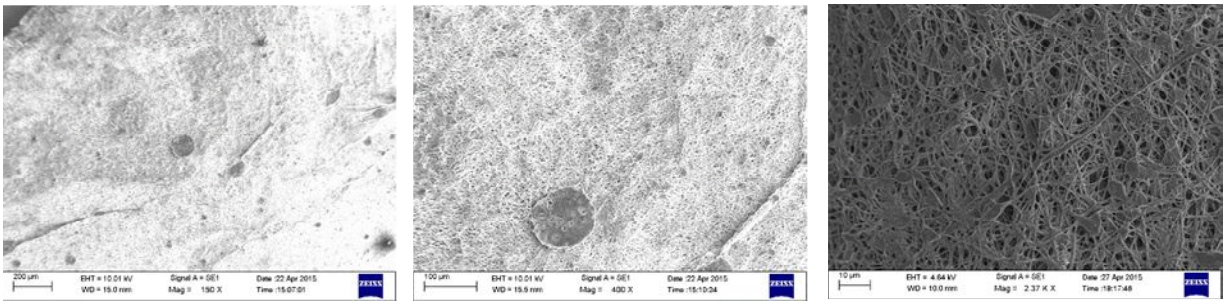

(a) (b) (c)

Figure 3.3: Scanning Electron Micrographs of PCL - MMP-1 at (a) 150X (b) 400X and (c) 2K

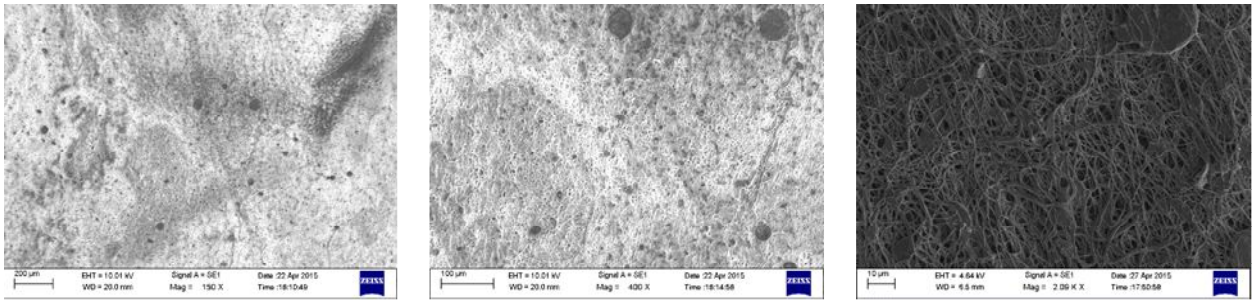

(a) (b) (c)

Figure 3.4: Scanning Electron Micrographs of PCL - Elastase at (a) 150X (b) 400X and (c) 2K

Figure 3.5 displays the SEM micrographs of electrospun PDO fiber mats at 150X, 400X and 2K magnification. Fiber diameter for PDO was determined to be 4.42 µm. Figure 3.6 displays the SEM micrographs of crimped PDO fiber mats at 150X, 400X and 2K magnification. The fiber diameter for crimped PDO was determined to be 7.88 µm

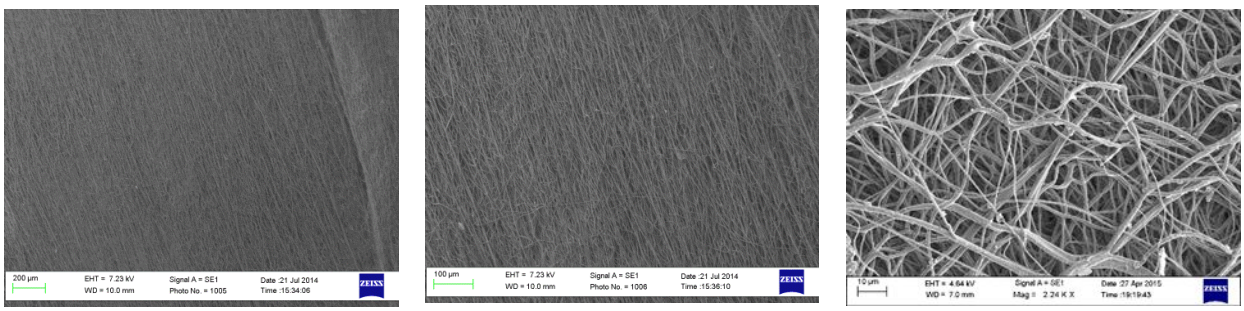

(a) (b) (c)

Figure 3.5: Scanning Electron Micrographs of PDO at (a) 150X (b) 400X and (c) 2K

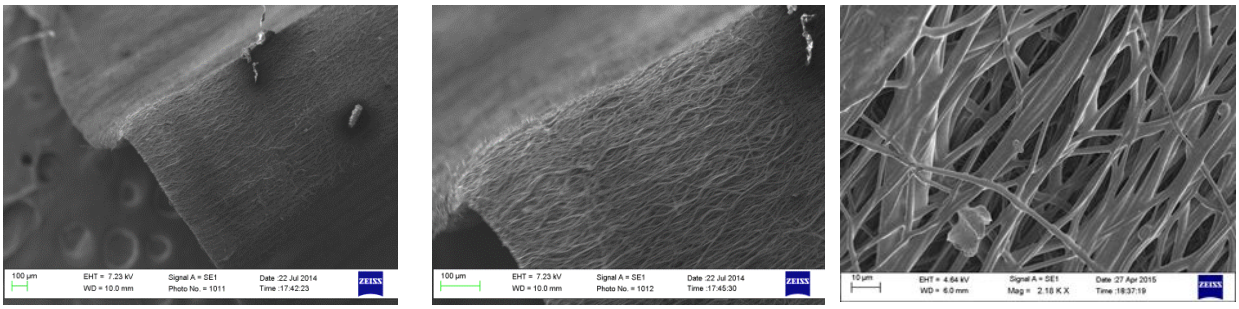

(a) (b) (c)

Figure 3.6: Scanning Electron Micrographs of crimped PDO at (a) 150X (b) 400X and (c) 2K

Figure 3.7 displays the SEM micrographs of PDO fibers after being incubated with MMP-1 solution at three different magnifications, 150X, 400X and 2K. Fiber diameter was determined to be 5.78 µm, after incubation with MMP-1. Figure 3.8 displays the SEM micrographs of PDO fibers after being incubated with Elastase solution at three different magnifications 150X, 400X and 2K. Fiber diameter was determined to be 1.60µm, after incubation with Elastase. The incubation of PDO in MMP-1 resulted in a slight increase in fiber diameter, and a significant decrease in fiber diameter when incubated with Elastase. The greater degradation and fiber diameter increase is possibly due to doping of MMP-1 within the fibers, while the fiber diameter decrease for Elastase shows greater degradation of the ether – ester bonds by Elastase.

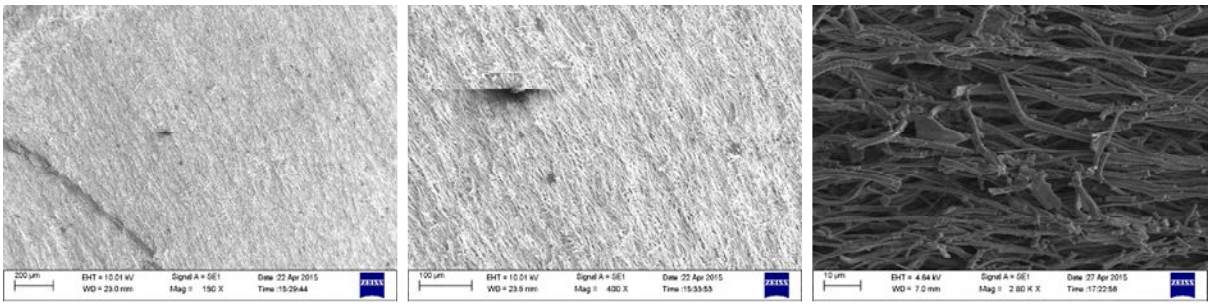

(a) (b) (c)

Figure 3.7: Scanning Electron Micrographs of PDO – MMP-1 at (a) 150X (b) 400X and (c) 2k

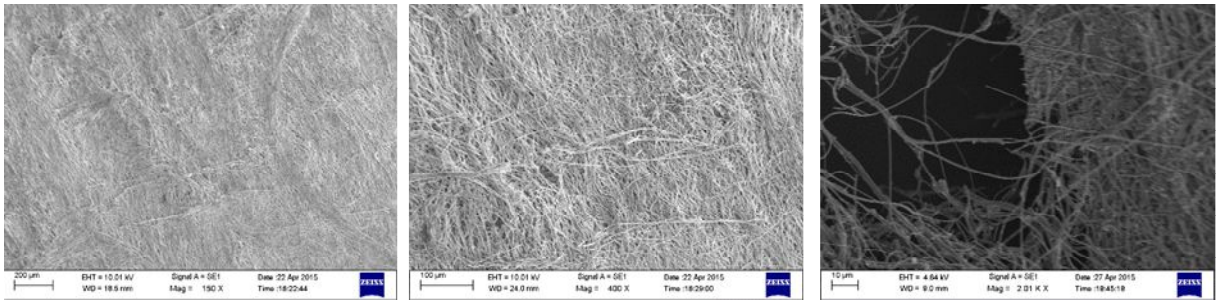

(a) (b) (c)

Figure 3.8: Scanning Electron Micrographs of PDO – Elastase at (a) 150X (b) 400X and (c) 2K

Figure 3.9 displays the SEM micrographs of electrospun Tecoflex™ EG 80A fiber mats at 150X, 400X and 2K magnification. Fiber diameter for Tecoflex™ EG 80A was determined to be 9.99 µm. Figure 3.10 displays the SEM micrographs of crimped Tecoflex™ EG 80A fiber mats at 150X, 400X and 2K magnification. Fiber diameter for crimped Tecoflex™ EG 80A was determined to be 3.29 µm.

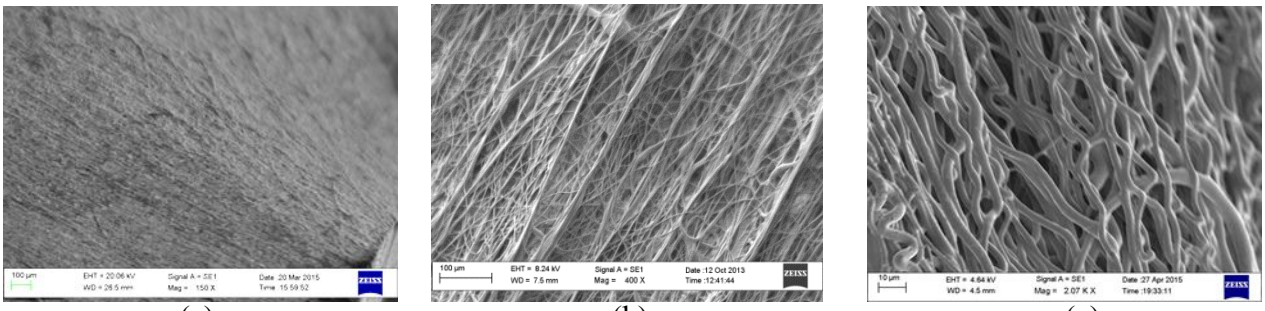

(a) (b) (c)

Figure 3.9: Scanning Electron Micrographs of Tecoflex™ EG 80A at (a) 150X (b) 400X and (c) 2K

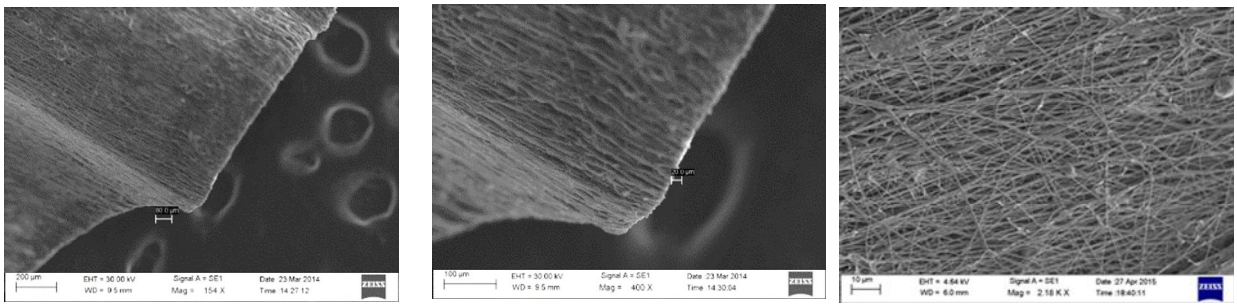

(a) (b) (c)

Figure 3.10: Scanning Electron Micrographs of crimpred Tecoflex™ EG 80A at (a) 150X (b) 400X and (c) 2K

Figure 3.11 displays the SEM micrographs of Tecoflex™ EG 80A fibers after being incubated with MMP-1 solution at three different magnifications, 150X, 400X and 2K. Fiber diameter for Tecoflex™ EG 80A after incubation with MMP-1 was determined to be 1.00 µm. Figure 3.12 displays the SEM micrographs of Tecoflex™ EG 80A fibers after being incubated with Elastase solution at three different magnifications, 150X, 400X and 2K. Fiber diameter for Tecoflex™ EG 80A after incubation with Elastase was determined to be 21.30µm.

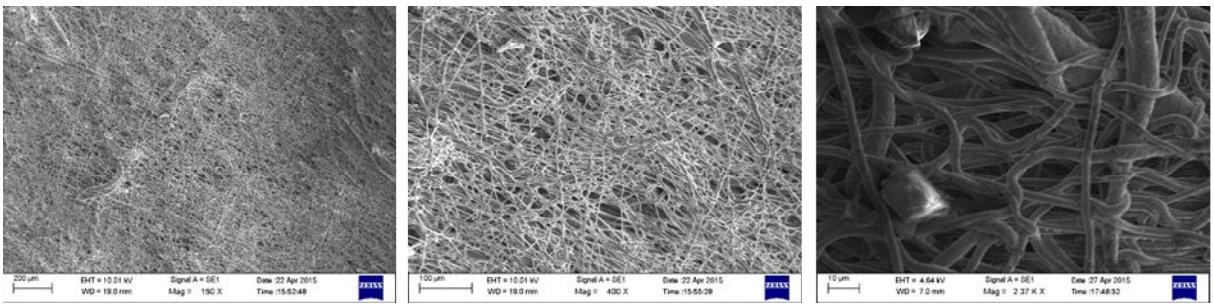

(a) (b) (c)

Figure 3.11: Scanning Electron Micrographs of Tecoflex™ EG 80A – MMP-1 at (a) 150X (b) 400X and (c) 2K

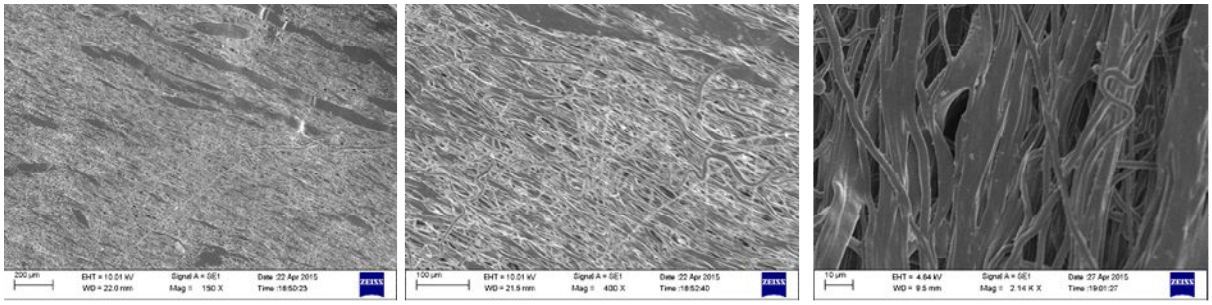

(a) (b) (c)

Figure 3.12: Scanning Electron Micrographs of Tecoflex™ EG 80A – Elastase at (a) 150X (b) 400X and (c) 2K

Figure 3.13 displays the SEM micrographs of electrospun Carbothane™ 3575A fiber mats at 150X, 400X and 2K magnification. Fiber diameter for Carbothane™ 3575A was determined to be 16.93µm. Figure 3.14 displays the SEM micrographs of crimped Carbothane™ 3575A fiber mats at 150X, 400X and 2K magnification. Fiber diameter for crimped Carbothane™ 3575A was determined to be 9.15µm

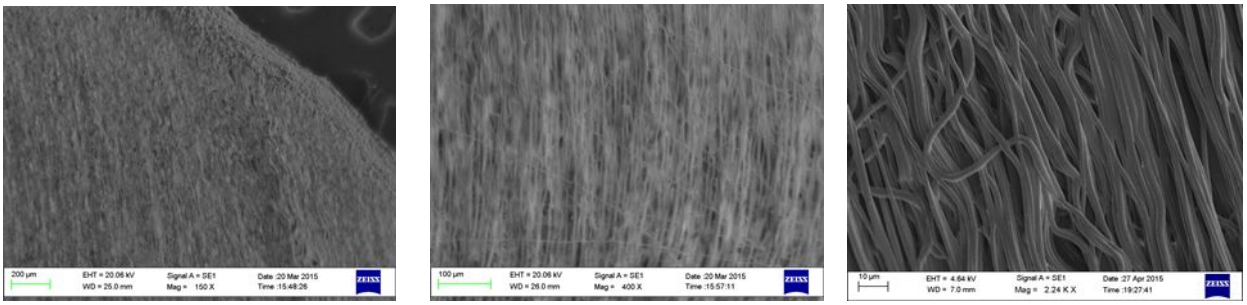

(a) (b) (c)

Figure 3.13: Scanning Electron Micrographs of Carbothane™ 3575A at (a) 150X (b) 400X and (c) 2K

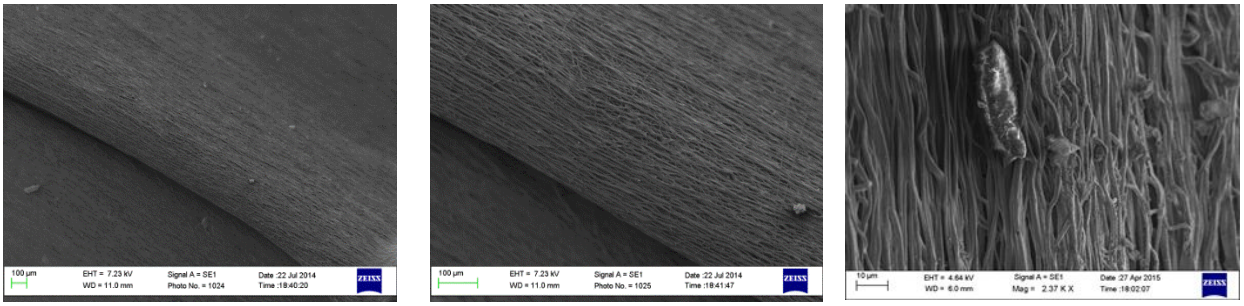

(a) (b) (c)

Figure 3.14: Scanning Electron Micrographs of crimped Carbothane™ 3575A at (a) 150X (b) 400X and (c) 2K

Figure 3.15 displays the SEM micrographs of Carbothane™ 3575A fibers after being incubated with MMP - 1 solution at three different magnifications,150X, 400X and 2K. Fiber diameter for Carbothane™ 3575A after incubation with MMP-1 was determined to be 8.71µm. Figure 3.16 displays the SEM micrographs of Carbothane™ 3575A fibers after being incubated with Elastase solution at three different magnifications, 150X, 400X and 2K. Fiber diameter for Carbothane™ 3575A after incubation with Elastase was determined to be 8.54µm.

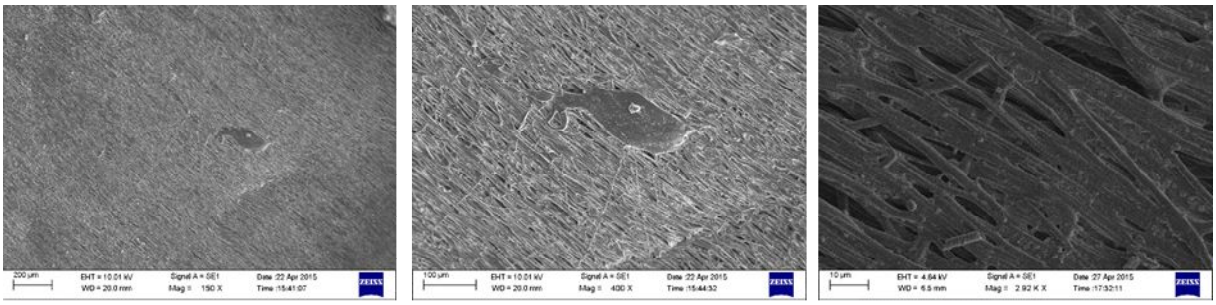

(a) (b) (c)

Figure 3.15: Scanning Electron Micrographs of Carbothane™ 3575A – MMP-1 at (a) 150X (b) 400X and (c) 2K

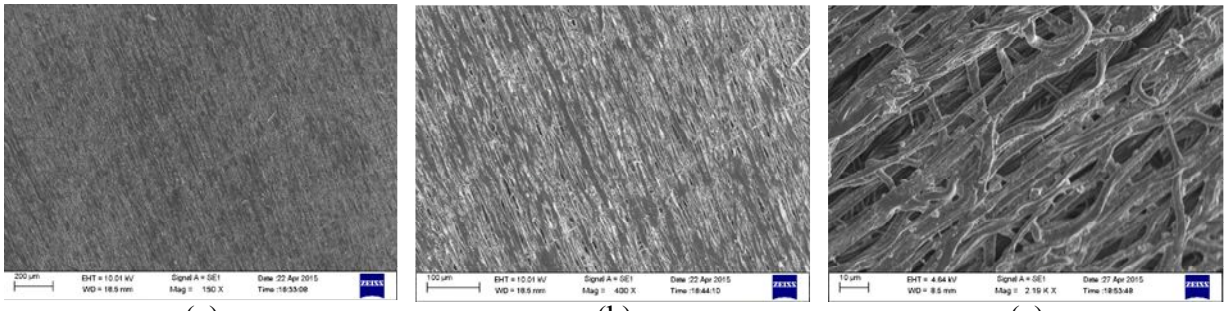

(a) (b) (c)

Figure 3.16: Scanning Electron Micrographs of Carbothane™ 3575A – Elastase at (a) 150X (b) 400X and (c) 2K

Scanning Electron Microscopy of Twisted PCL and PDO

Figure 3.17 displays the SEM micrographs of twisted PCL strands at 150X, 400X and 2K magnification. Fiber diameter for the PCL twisted strands was determined to be 4.83µm. Figure 3.18 displays the SEM micrographs of twisted PDO strands at 150X, 400X and 2K magnification. Fiber diameter for the PDO twisted strands was determined to be 3.85µm.

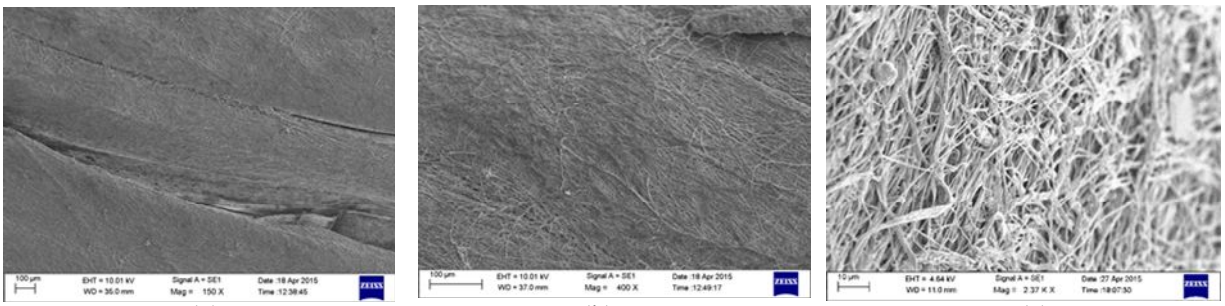

(a) (b) (c)

Figure 3.17: Scanning Electron Micrographs of twisted PCL at (a) 150X (b) 400X and (c) 2K

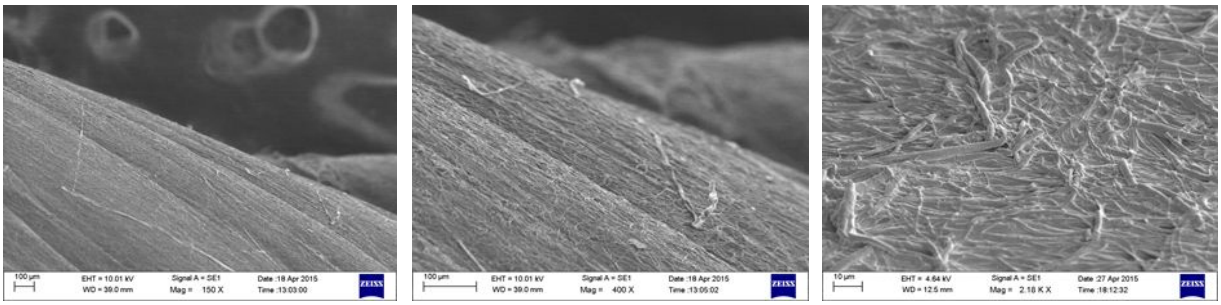

(a) (b) (c)

Figure 3.18: Scanning Electron Micrographs of twisted PDO at (a) 150X (b) 400X and (c) 2K

Tensile Testing

Tensile strength testing is one of the simplest, most fundamental types of mechanical test that can be performed on a sample. Tensile testing will allow the quick determination of how a material will react to the forces being applied in tension. Tensile strength analysis will give a complete tensile profile of the material including maximum load, tensile stress at maximum load, Young's Modulus and tensile strain. Tensile strength analysis of flexible materials, such as polymer mats, must follow the established ASTM D882 standards.

Mechanical tensile strength testing was performed for every sample conducted in this study. The data was invaluable in providing insight into the specific properties of each sample. The most widely used mechanical test is one that measures stress at a constant strain rate, ultimate tensile stress and strain ruptures will vary depending on temperature and rate of strain. Any amorphous polymer that is stretched undergoes some orientation of polymer segments. In their oriented state, crystallization may occur, which will increase the effective number of cross-links[47]. When the amorphous polymer is subject to the process of orientation by stretching, also known as drawing out, rearrangement of the polymer chains often takes place. The orientated polymers chains are oriented in the direction of the stress, they give high strength and low elongation in the direction of the fiber axis.[47] If crystallization does not occur, the behavior of the sample to rupture will be the same as with small deformations.[47] Figure 4.1 describes the main types of stress-strain curves of four of the most common polymer materials.

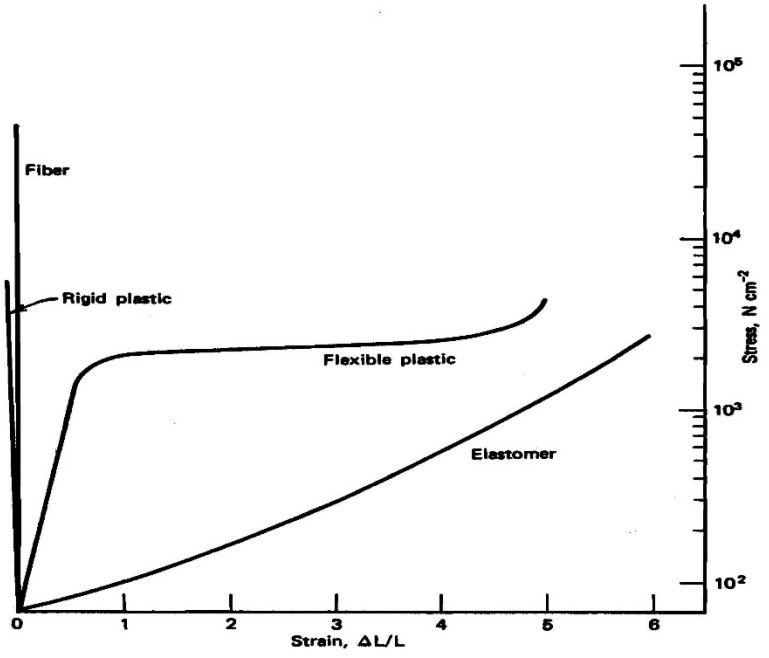

Figure 4.1: Stress–strain plots for a typical elastomer, flexible plastic, rigid plastic, and fiber. [48]

Most polymer materials will behave in the following ways; a soft and weak material will have a low modulus, a low yield stress and a moderate to high elongation at the break point. Yield refers to a point where the material starts to experience a deformation but the material can still continue to deform and absorb energy beyond that point until it finally breaks. A hard and brittle material will have a high modulus and a low elongation at break; it may not yield before breaking. A soft but tough material will have a low modulus but have a high elongation and high stress at break, it may have a low yield stress. A hard and strong material will have a high modulus, high yield stress, and high breaking stress and perhaps a moderate elongation at break. Lastly, a hard and tough material will have a high modulus, high elongation, and high stress at break.[47] Table 3.1 shows a condensed comparison of reported ACL mechanical properties.

	Maximum Load (N)	Tensile Stress at Maximum Load (MPa)	Young's Modulus (MPa)	Energy at Max. Load (N-m)	Strain at Max. Stress (%)
Human ACL (16-26 Yrs.)	1725 ± 269*	37.8 ± 9.3 MPa	111 ± 26 MPa	12.8 ± 5.5	30 ± 10.0
Human ACL (48-86 Yrs.)		13.3 ± 5.0 MPa	65.3 ± 24.0 MPa	4.89 ± 2.36	44.3 ± 8.5
Collagen		5 – 500 MPa	100 – 2900 MPa		

Table 3.1: Comparison of Mechanical Properties
*** Value not age specific [49]**

The values for human ACL as reported by Noyes and Grood have been shown to vary with age, the reported average ultimate tensile stress (tensile stress) of 37.8 ± 9.3 MPa, a Young's modulus of 111 ± 26 MPa and failure strain of 60.25 ± 6.78%, for human donor ages 16 to 26 years old. For human donors aged 48 to 86 years old, the average tensile stress is 13.3 ± 5.0 MPa,

a Young's modulus of 65.3 ± 24.0 MPa and a failure strain of 48.5 ± 11.9%.[50] Collagen one of the most abundant components of native tissue has a Young's modulus that ranges from 100 to 2900 MPa [51], tensile stress for collagen ranges from 5 to 500MPa. [51] Thomas et al, have reported the following for aligned nanofibrous scaffolds of PCL fabricated by electrospinning; for PCL spun between 3000 rpm to 6000 rpm the average ultimate tensile strength ranged between 4.21 ± 0.35 MPa to 9.58 ± 0.71 MPa. The average tensile modulus increased with rotational speed with 11.93 ± 1.22 MPa for PCL at 3000 rpm and 33.20 ± 1.98 MPa for PCL at 6000 rpm.[45]

Figure 4.2 represents the tensile testing of PCL for 10 individual samples. Table 3.1 presents the mean and standard deviations of PCL tensile testing, which resulted in having a Young's Modulus average of 247.23 ± 32.70 MPa, an average stress of 82.66 ± 14.38 MPa, and an average strain of 0.68 ± 0.055 mm/mm. The PCL scaffolds produced for this research are stiffer than reported, this could be due to a lack of hydration on the scaffolds that could be causing the ester bonds to crystallize more effectively and pack closer to each other; therefore, making the material more brittle. Another example that this PCL has become brittle is shown in its very low extension, which only averages 0.68 mm/mm compared to the reported ultimate strain for aligned PCL, which ranged from 80 % to 190%.[45] However, when compared to the mechanical properties of two major structural components found in soft tissues, collagen and elastin, the Young's modulus and tensile stress for PCL are still within the ranges of reported collagen values. It can be said that for mechanical properties the single layer PCL scaffolds produced in this research, are closer in nature to the mechanical properties of native collagen.

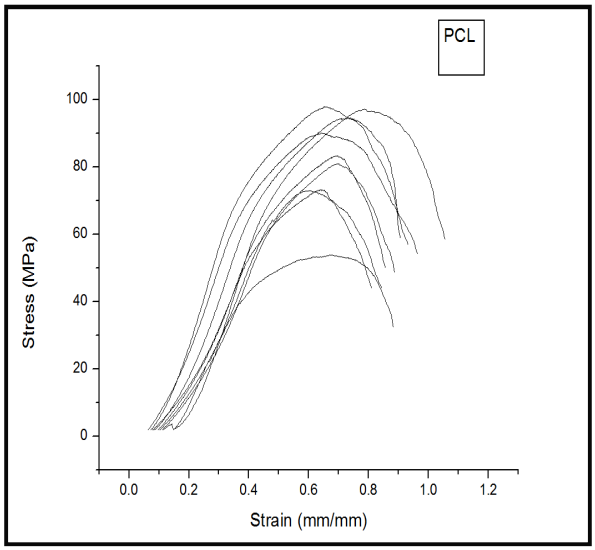

Figure 4.2: Tensile testing of individual PCL

Maximum Load ± Std. Deviation (N)	Tensile Stress at Maximum Load ±Std.Deviation (MPa)	Modulus (Automatic Young's) ±Std.Deviation (MPa)	Tensile Strain (Extension) at Maximum Load ±Std. Deviation (mm/mm)	Energy at Maximum Load ± Std.Deviation (N-mm)
2.27 ± 0.39	**82.66 ± 14.38**	**247.23 ± 32.70**	**0.68 ± 0.055**	**5.90 ± 1.45**

Table 3.2: Mean and standard deviations of PCL tensile testing

Figure 4.3 represents the tensile testing of crimped PCL for 10 individual samples. Table 3.2 presents the mean and standard deviations of crimped PCL tensile testing, which resulted in having a Young's modulus average of 373.44 ± 80.63 MPa, an average stress of 113.19 ± 26.13 MPa, and an average strain of 0.72 ± 0.12 mm/mm. When compared to uncrimped PCL nanofibers, crimped PCL fibers show an increase in both Young' modulus, tensile stress and extension. The Young's modulus is now an average of 373.44 ± 80.63 MPa, indicating that the material has become quite stiff, in comparison to values reported by Thomas et al. Tensile stress for crimped PCL fibers shows a 26 MPa increase, from 82.66 ± 14.38 MPa to an average of

113.19 ± 26.13 MPa. Crimped PCL has a slight increase in extension with an average of 0.72 mm/mm compared to 0.65 mm/mm for uncrimped PCL fibers. Both the Young's modulus and tensile stress for crimped PCL are still within the ranges of reported collagen values. The crimped PCL fibers are an even stiffer material but somehow it is less brittle than uncrimped PCL.

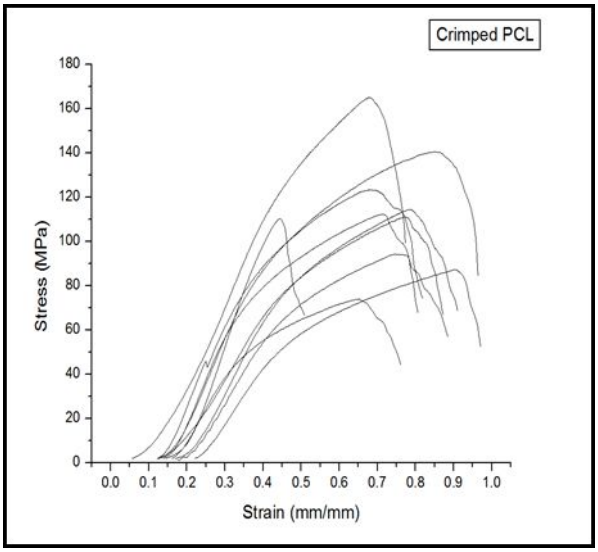

Figure 4.3: Tensile testing of individual crimped PCL

Maximum Load ± Std. Deviation (N)	Tensile Stress at Maximum Load ±Std.Deviation (MPa)	Modulus (Automatic Young's) ±Std.Deviation (MPa)	Tensile Strain (Extension) at Maximum Load ±Std. Deviation (mm/mm)	Energy at Maximum Load ± Std.Deviation (N-mm)
3.11 ± 0.71	**113.19 ± 26.13**	**373.44 ± 80.63**	**0.72 ± 0.12**	**8.30 ± 2.95**

Table 3.3: Mean and standard deviations of crimped PCL tensile testing

One theory that attempts to explain the effects of polymer crimping is the microhardness theory. In a paper written by Calleja [52], he explains that when polymers are subject to crimping indentations, the lamellae of the original structure experience a local irreversible mechanism of fracture into smaller units.[52] The heat generated during lamellae destruction provides sufficient chain mobilization in the polymer blocks that allow them to rearrange to a new thickness[52]; during crimping there is also external heat being applied, providing more energy for the chains to rearrange. Volume of crystals displaced will increase inversely proportional to the volume of material destroyed, when a constant applied load P, is excerted.[52] PCL was placed under an applied pressure, (the crimping apparatus), for two hours, at 55°C. The melting point of PCL ranges between 59 to 64 °C [27], 55°C was chosen as a median temperature to prevent melting of the PCL scaffolds. The volume of crystals displaced will be larger in softer materials; smaller crystalline blocks increase the volume of material displacement. More recrystallizations will occur in with increasing volume displacement, leading to a stiffer material. PCL itself contains a small C_6H_{10} group as the soft segment. Therefore it can be said that, larger recrystallizations, due to an increase in pressure and heat, occurred in the crimped PCL samples, as shown by its increasing stiffness.

In matters of explaining greater extension for the crimped PCL samples vs. uncrimped, we must consider the effect of the actual crimping itself. Human ACL ligaments themselves exhibit this crimped pattern, and what allows the ACL ligament to withstand all those small everyday stress forces, such as bending the knee, going up/down stairs, walking, jogging etc. Crimping allows for only partial use of the fibers, only those that are necessary to sustain a small strain. Full use of all the fibers will be exhibited when there is a larger load and possibly to fiber failure.

Once the fibers have become crimped in nature, they will experience a longer area of low stress; this is indicative that the crimped fibers are becoming fully extended as their load increases. In this area of low stress, or "toe region", the crimping pattern has been distributed evenly throughout the polymer sample, such that when the polymer sample is pulled in tension, individual fibers are recruited and elongated as the force is increased; full recruitment and uncrimping of individual fibers will result in the beginning of the linear region, exemplified by a larger linear stiffness.[9] In the case of the crimped PCL samples, this can be seen in its slightly longer extension but increased Young's Modulus.

Figure 4.4 represents the tensile testing of PDO for 10 individual samples. Table 3.3 presents the mean and standard deviations of PDO tensile testing, which resulted in having a Young's modulus average of 274.73 ± 73.64 MPa, an average stress of 56.58± 14.74 MPa, and an average strain of 0.45 ± 0.07 mm/mm. These values are different those reported in the literature for nanofibrous scaffolds of PDO fabricated by electrospinning. Various articles have reported the average ultimate tensile strength of PDO to range from 1.7 to 12 MPa, the average tensile modulus for PDO is reported between 2 to 46 MPa and extension reaching from 31 to 240%. [51, 53] The PDO scaffolds produced for this research are once again stiffer than reported, this could also be due to a lack of hydration on the scaffolds, maximizing the ether- ester bonds ability to crystallize more effectively and pack closer to each other, therefore, making the material more brittle. Previously cited sources do not indicate if the fibers were aligned. In the study conducted by Thomas et al, it was reported that when rotational speed was increased, orientation and alignment of the fibers increased, leading to increased tensile stress but shrinkage in strain.[45] Higher rotational speeds have been shown to decrease the space in between fibers, due to an extra

stretching of the fibers at higher uptake rates.[45] This allows the polar ether-ester bonds to come closer improving their ability for intermolecular hydrogen bonding; resulting in glassy or crystalline phases that impart toughness on the material. An increase in brittleness is exhibited by PDO in its extremely low extension, which only averages 0.45 mm/mm compared to the reported ultimate strain which ranged from 31 % to 240 %. However, both the Young's modulus and tensile stress for PDO are still within the ranges of reported collagen values. It can be said that the mechanical properties of these, our single layer PDO scaffolds are also closer in nature to the mechanical properties of native collagen.

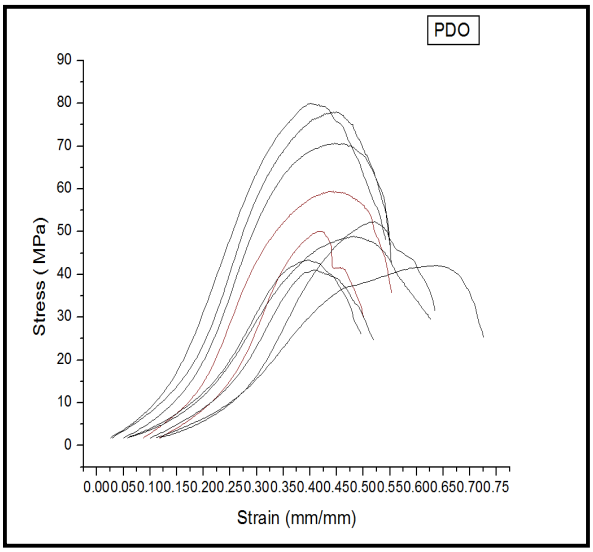

Figure 4.4: Tensile testing of individual PDO

Maximum Load ± Std. Deviation (N)	Tensile Stress at Maximum Load ±Std.Deviation (MPa)	Modulus (Automatic Young's) ±Std.Deviation (MPa)	Tensile Strain (Extension) at Maximum Load ±Std. Deviation (mm/mm)	Energy at Maximum Load ± Std.Deviation (N-mm)
1.55 ± 0.40	**56.58 ± 14.74**	**274.73 ± 73.64**	**0.45 ± 0.072**	**2.23 ± 0.75**

Table 3.4: Mean and standard deviations of PDO tensile testing

Figure 4.5 represents the tensile testing of crimped PDO for 10 individual samples. Table 3.4 presents the mean and standard deviations of crimped PDO tensile testing, which resulted in having a Young's modulus average of 5.51 ± 3.20 MPa, an average stress of 9.11 ± 3.88 MPa, and an average strain of 5.24 ± 0.64 mm/mm. In the case of crimped PDO fibers the data is surprisingly consistent with reported literature values. Both the average Young's modulus and tensile stress fall within the ranges of the literature data. Crimped PDO samples had one of the longest extension averages within our samples, at 5.24 mm/mm. This is also consistent with PDO reporting the longest strain at break ranging from 31% to 240%. Crimped PDO behaves as would be expected of a crimped scaffold with a longer extension and a lower modulus, thereby making it more elastic and less rigid, however it also lowers its tensile stress to around 9 MPa compared to the 56 MPa of the uncrimped PDO fibers. PDO samples were under applied pressure for 2 hours at 85°C. The melting point of PDO ranges between 110 to 115 °C, 85°C was deemed hot enough to set the crimping pattern and have no risk of melting. In this case, the crimping effect can be seen in the larger extension of the crimped PDO fibers, it does not account for the decreased stiffness.

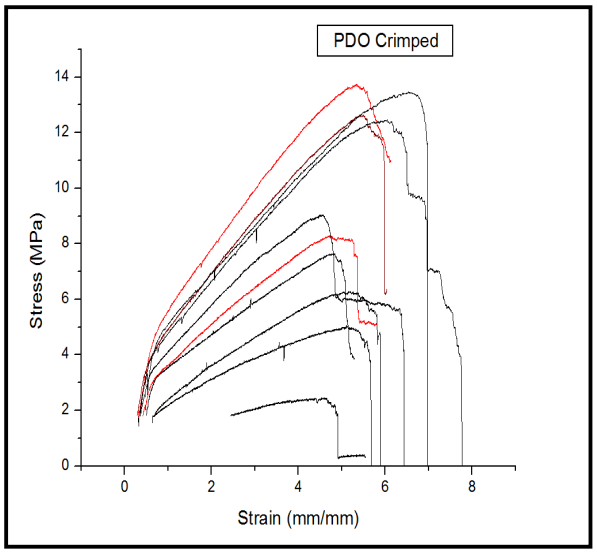

Figure 4.5: Tensile testing of individual crimped PDO

Maximum Load ± Std. Deviation (N)	Tensile Stress at Maximum Load ±Std.Deviation (MPa)	Modulus (Automatic Young's) ±Std.Deviation (MPa)	Tensile Strain (Extension) at Maximum Load ±Std. Deviation (mm/mm)	Energy at Maximum Load ± Std.Deviation (N-mm)
0.25 ± 0.10	**9.11 ± 3.88**	**5.51 ± 3.20**	**5.24 ± 0.64**	**6.44 ± 3.47**

Table 3.5: Mean and standard deviations of crimped PDO tensile testing

Comparing the mechanical properties of our PCL and crimped PCL scaffolds to previously reported mechanical properties. It can be said that they do not have all the mechanical properties of the native human ACL tissue, in most cases the Young's modulus is too high and the tensile stress is too low. They do not behave as other aligned scaffolds which have been reported high speeds, and they do not meet the standard for grafts that have been previously cited. The PCL samples behave as hard and brittle materials with high moduli and low elongations at break. The PCL samples do exhibit some of the mechanical properties matching those of native collagen tissue. The same can be observed of the regular PDO samples, they only share some mechanical

properties of native collagen tissue and it behaves as a hard and brittle material. Crimped PDO behaves as other previously electrospun PDO nanofibers, but its mechanical properties are lower than those of human ACL, native collagen tissue and do not meet the standards for grafts. Crimped PDO samples are the only ones so far that behave as a soft but tough material that has a low modulus, high elongation but low tensile stress.

Figure 4.6 represents the tensile testing of Tecoflex™ EG 80A for 10 individual samples. Table 3.5 presents the mean and standard deviations of Tecoflex™ EG 80A tensile testing, which resulted in having a Young's modulus average of 35.13 ± 9.39 MPa, an average stress of 49.92 ± 16.07 MPa, and an average strain of 2.49 ± 0.64 mm/mm. In the published data for Tecoflex EG 80A, [55] pure electrospun Tecoflex™ EG 80A nanofibers, have a Young's modulus average of 4.9 ± 1.2 MPa. The average breaking stress is 26 ± 5 MPa and the average extension is of 9.0 ± 0.1 mm/ mm. In this study, Tecoflex™ EG 80A has a higher Young's modulus and a higher breaking stress, making the material slightly harder; also it has a lower strain (extension) of only 2.49 mm/mm, compared to literature values of 9.0 mm/mm.[55] The study by Thomas et al, reports the effect of alignment at higher rotational rates such as the ones used in this research. Tecoflex™ EG 80A fibers were spun at 5000 rpm in this study, previously cited sources do not indicate if the fibers were aligned. Higher rotational speeds have been shown to decrease the space in between fibers, due to an extra stretching of the fibers at higher uptake rates.[45] This allows the hard segments in Tecoflex™ EG 80A, which in this case are the alicyclic diisocyanates, to come closer together improving their ability for intermolecular hydrogen bonding; resulting in glassy or crystalline phases that impart toughness on the material.

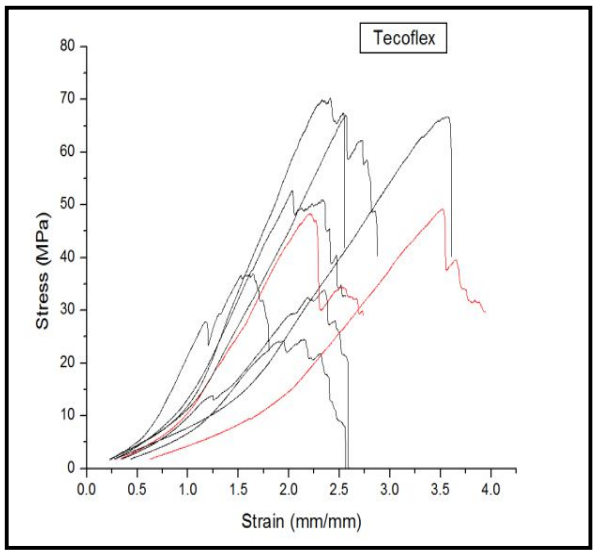

Figure 4.6: Tensile testing of individual Tecoflex

Maximum Load ± Std. Deviation (N)	Tensile Stress at Maximum Load ±Std.Deviation (MPa)	Modulus (Automatic Young's) ±Std.Deviation (MPa)	Tensile Strain (Extension) at Maximum Load ±Std. Deviation (mm/mm)	Energy at Maximum Load ± Std.Deviation (N-mm)
1.37 ± 0.44	**49.92 ± 16.07**	**35.13 ± 9.39**	**2.49 ± 0.64**	**10.04 ± 8.55**

Table 3.6: Mean and standard deviations of Tecoflex™ EG 80A tensile testing

Figure 4.7 represents the tensile testing of crimped Tecoflex™ EG 80A for 10 individual samples. Table 3.6 presents the mean and standard deviations of crimped Tecoflex™ EG 80A tensile testing, which resulted in having a Young's modulus average of 20.96 ± 1.96 MPa, an average stress of 57.52 ± 15.58 MPa, and an average strain of 3.69 ± 0.70 mm/ mm. Crimped Tecoflex™ EG 80A has a lower Young's modulus than uncrimped Tecoflex™ EG 80A but has a higher stress and a slightly higher extension than uncrimped Tecoflex™ EG 80A. Compared to the reported literature values, its Young's modulus and stress are higher but once again the extension is shorter compared to the 9.0 mm/mm reported.[55] The increase in extension for the

crimped fibers can be explained due to the crimping factor that allows crimped fibers to extend longer. The microhardness theory can be used to explain the effect of heat and pressure on the crimped Tecoflex™ EG 80A samples, as it did for crimped PDO. Tecoflex™ EG 80A samples were submitted to pressure and high heat of 95 °C for about two hours, while Tecoflex™ EG 80A has a high melting point at 182°C,[56] so it should be feasible to crimp Tecoflex™ EG 80A with no danger of melting the scaffolds. It could be said that for crimped Tecoflex™ EG 80A the applied heat and pressure caused the already highly crystalline alicyclic diisocyantes to break and reform into smaller, softer Tecoflex™ EG 80A segments. The crimped waves that result from the crimping process do help to give this sample more elasticity under stress and we see this effect occurring with crimped Tecoflex™ EG 80A. That would explain how crimped Tecoflex™ EG 80A exhibits more elastic behavior with less rigidity than regular Tecoflex™ EG 80A.

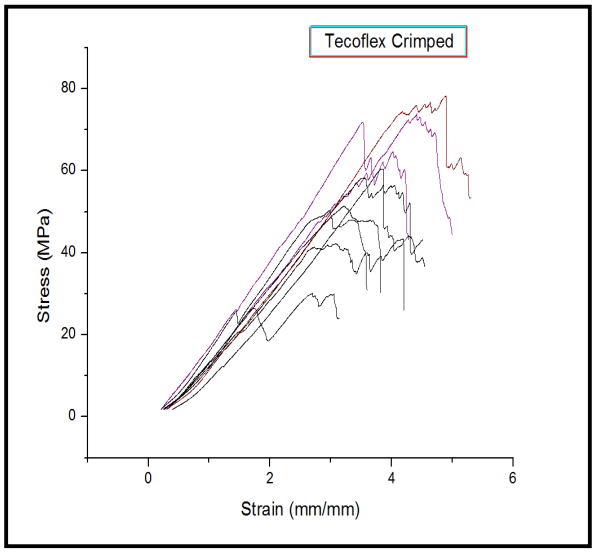

Figure 4.7: Tensile testing of individual crimped Tecoflex™ EG 80A

Maximum Load ± Std. Deviation (N)	Tensile Stress at Maximum Load ±Std.Deviation (MPa)	Modulus (Automatic Young's) ±Std.Deviation (MPa)	Tensile Strain (Extension) at Maximum Load ±Std. Deviation (mm/mm)	Energy at Maximum Load ± Std.Deviation (N-mm)
1.58 ± 0.42	**57.52 ± 15.58**	**20.96 ± 1.96**	**3.69 ± 0.70**	**22.04 ± 9.17**

Table 3.7: Mean and standard deviations of crimped Tecoflex™ EG 80A tensile testing

Figure 4.8 represents the tensile testing of Carbothane™ 3575A for 10 individual samples. Table 3.7 presents the mean and standard deviations of Carbothane™ 3575A tensile testing, which resulted in having a Young's modulus average of 1.91 ± 0.44 MPa, an average stress of 7.65 ± 2.22 MPa, and an average strain of 5.68 ± 0.97 mm/mm. Data published recently, as well as published by the Lubrizol company put the average tensile stress of Carbothane™ 3575A at around the 11.40 ± 0.9 MPa range.[38,57] Carbothane™ 3575A in this study, has slightly lower values, indicating that in this case the material is soft and weak. This could be due to Carbothane™ 3575A being a less rigid polymer, from what we know of the structure it does not seem to contain any aromatic rings or carbonyls and the structure seems for the most part alicyclic in nature. The lack of aromatic and carbonyls limit the formation of intermolecular hydrogen bonding sites. Carbothane™ 3575A shows the longest extension out of all our samples at 5.68 mm/mm, a high elongation is a characteristic of soft and weak materials which possess low modulus, low tensile stress and a moderate to high extension. [33]

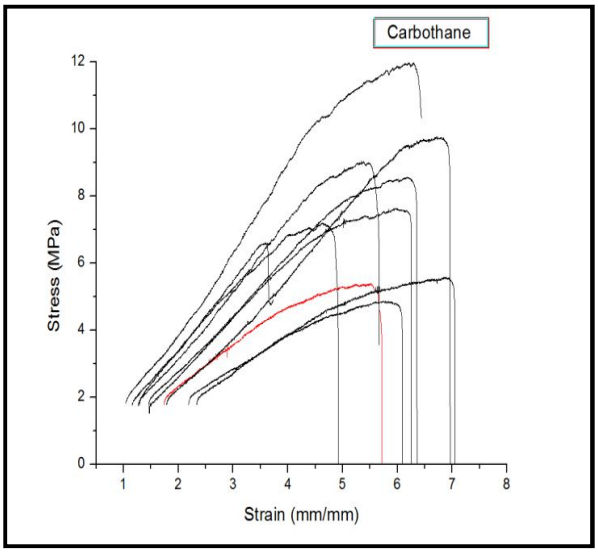

Figure 4.8: Tensile testing of individual Carbothane™ 3575A

Maximum Load ± Std. Deviation (N)	Tensile Stress at Maximum Load ±Std.Deviation (MPa)	Modulus (Automatic Young's) ±Std.Deviation (MPa)	Tensile Strain (Extension) at Maximum Load ±Std. Deviation (mm/mm)	Energy at Maximum Load ± Std.Deviation (N-mm)
0.21 ± 0.06	**7.65 ± 2.22**	**1.91 ± 0.44**	**5.68 ± 0.97**	**4.49 ± 1.79**

Table 3.8: Mean and standard deviations of Carbothane™ 3575A tensile testing

Figure 4.9 represents the tensile testing of crimped Carbothane™ 3575A for 10 individual samples. The graphs display the Young's modulus, tensile stress, and tensile strain exhibited by crimped Carbothane™ 3575A. Table 3.8 presents the mean and standard deviations of crimped Carbothane™ 3575A tensile testing, which resulted in having a Young's modulus average of 3.86 ± 0.75 MPa, an average stress of 14.84 ± 3.76 MPa, and an average strain of 4.89 ± 1.39 mm/mm. The values for crimped Carbothane™ 3575A are slightly higher than for uncrimped Carbothane™ 3575A, indicating an increase in crystallinity. The average stress is slightly higher for our crimped Carbothane™ 3575A at 14.84 Mpa compared to the reported average of 11.40

MPa, this could be due to a lack of hydration in the scaffolds as well as in increase in crystallinity. During crimping Carbothane™ 3575A was subject to very low heat only 35°C but the applied pressure for 2 hours can still be causing a rearrangement in crystallinity, causing the material to become harder. Even though the reported melting point for Carbothane™ 3575A is 215°C [58], the scaffolds that were crimped during this research showed complete melting at any temperature higher than 50°C. Crimped Carbothane™ 3575A has also become slightly more brittle than its uncrimped Carbothane counterpart, due to a slight decrease in elongation, the crimping has made the material slightly brittle.

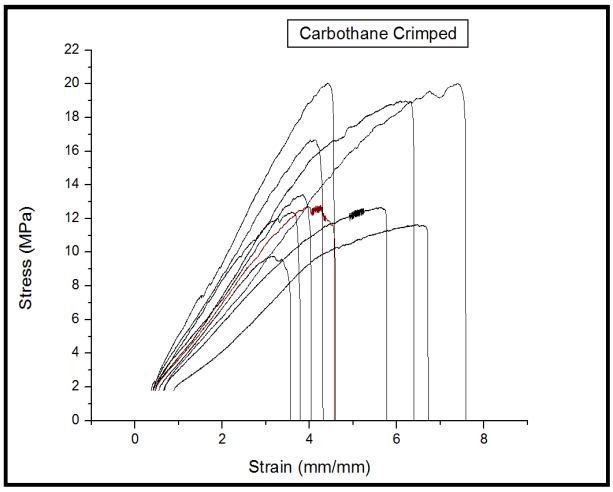

Figure 4.9: Tensile testing of individual crimped Carbothane™ 3575A

Maximum Load ± Std. Deviation (N)	Tensile Stress at Maximum Load ±Std.Deviation (MPa)	Modulus (Automatic Young's) ±Std.Deviation (MPa)	Tensile Strain (Extension) at Maximum Load ±Std. Deviation (mm/mm)	Energy at Maximum Load ± Std.Deviation (N-mm)
0.40 ±0.10	14.84 ± 3.76	3.86 ± 0.75	4.89 ± 1.39	8.56 ± 4.15

Table 3.9: Mean and standard deviations of crimped Carbothane™ 3575A tensile testing

Comparing the mechanical properties of Tecoflex™ EG 80A and crimped Tecoflex™ EG 80A scaffolds to previously reported mechanical properties. Both, regular and crimped Tecoflex™ EG 80A exhibit a tensile stress within the range of the native human ACL tissue when taking the standard deviations into account. The Young's moduli of Tecoflex™ EG 80A scaffolds however, are lower those reported for human ACL's and native collagen tissue. The tensile stress exhibited by both Tecoflex™ EG 80A scaffolds also fall within the range of the native collagen tissue of 5-500 MPa. The mechanical properties of both Tecoflex™ EG 80A scaffolds however, are higher than for those reported in previous studies conducted in this laboratory.[55] As a result of the scaffolds increased brittleness, their extension also suffers and is reported at only 2.49-3.69 mm/mm as opposed to the 9.0 mm/mm reported.[55] Neither of the Tecoflex™ EG 80A scaffolds meet the standard for grafts that have been previously cited. It can be concluded that our highly aligned crimped and uncrimped Tecoflex™ EG 80A scaffolds do not have the required mechanical properties to be considered suitable materials for tissue engineering applications. Both crimped and uncrimped Carbothane™ 3575A scaffolds do not fall into the range of any of the previously cited reported values for human ACL, native collagen or previously reported Carbothane™ 3575A fibers produced in this laboratory.[57] Crimped Carbothane™ 3575A showed increased crystallinity when compared to uncrimped Carbothane™ 3575A. Carbothane™ 3575A behaves as a soft and weak material that is characterized by a low modulus, low tensile stress and a moderate to high elongation.[43] It can be concluded that Carbothane™ 3575A has the weakest mechanical properties and is inadequate for high load bearing scaffolds.

Multilayered Tensile Testing

Based on the behavior of the single layered scaffolds, it was decided that PCL and PDO had the more suitable mechanical properties to continue to the next phase. The following results pertain only to PCL and PDO scaffolds that were multilayered using 1% beef gelatin.

Figure 5.1 represents the tensile testing of multilayered PCL for 10 individual samples. Table 4.1 presents the mean and standard deviations of multilayered PCL tensile testing, which resulted in having a Young's modulus average of 307 ±119 MPa, an average stress of 67.46 ± 28.69 MPa, and an average strain of 0.71 ± 0.19 mm/mm. Compared to our single layer PCL scaffolds, the multilayered scaffolds have lower tensile stress meaning the multilayered scaffolds are able to withstand less force. However, there was a slight increase in strain (extension) for the multilayered scaffolds compared to single layered PCL, as well as an increase in Young's modulus for the multilayered scaffolds. The decrease in tensile strength can be explained by analyzing the mechanical properties of beef gelatin, in a previous study conducted in this laboratory, beef gelatin was dissolved and electrospun. The mechanical properties of beef gelatin are weak, it has a maximum load of 0.15 N, a maximum tensile stress of 1.08 MPa, a Young's modulus of 14.77 MPa and a tensile strain (extension) of 0.20 (mm/mm).[59] In the study conducted by Garcia, it was shown that electrospun mixed scaffolds of PCL – beef resulted in lowered mechanical properties than those of PCL only scaffolds, the full results of those experiments can be found in Garcia's thesis which is referenced above.

From those results, we conclude that the beef gelatin is weakening our PCL scaffolds and bringing down its tensile stress and maximum load. The tensile strain is only slightly longer at 0.71 ± 0.19 (mm/mm) when compared to single layer PCL which has an extension of 0.68 ± 0.055 (mm/mm). It is possible that the multilayers are contributing slightly to longer extensions because more fibers are now available even when other fibers fail. An increase in Young's modulus is indicative of a smaller change in stiffness; when there is a low force accompanied by low extensions, this will result in a larger Young's modulus. PCL multilayered scaffolds exhibit this effect. One thing that could be contributing to stiffer multilayered scaffold could be the presence of collagen from the dissolved beef gelatin. This particular beef gelatin contains large amounts of carboxylic and amine groups, (further discussed in FTIR section), leading to increased hydrogen bonding within the PCL fibers, forming stronger and stiffer PCL nanofibers.

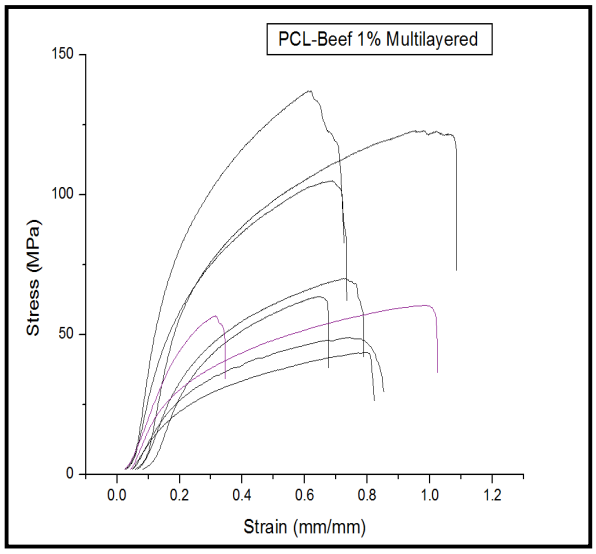

Figure 5.1: Tensile testing of individual multilayered PCL

Maximum Load ± Std. Deviation (N)	Tensile Stress at Maximum Load ±Std.Deviation (MPa)	Modulus (Automatic Young's) ±Std.Deviation (MPa)	Tensile Strain (Extension) at Maximum Load ±Std. Deviation (mm/mm)	Energy at Maximum Load ± Std.Deviation (N-mm)
1.85 ± 0.78	67.46 ± 28.69	307 ± 119	0.71 ± 0.19	6.83 ± 4.27

Table 4.1: Mean and standard deviations of multilayered PCL tensile testing

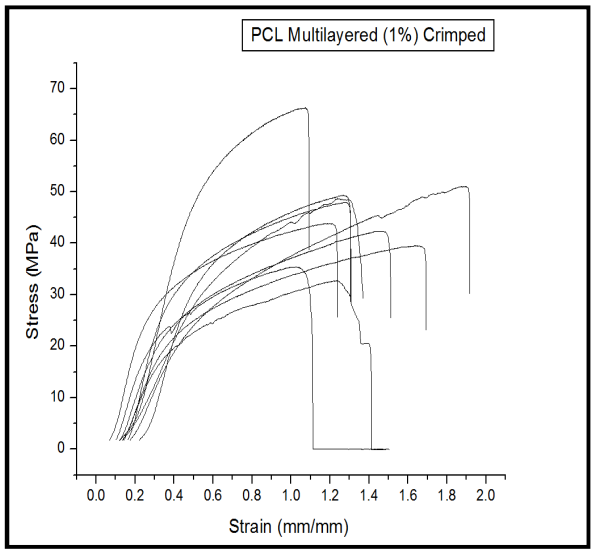

Figure 5.2: Tensile testing of individual crimped multilayered PCL

Maximum Load ± Std. Deviation (N)	Tensile Stress at Maximum Load ±Std.Deviation (MPa)	Modulus (Automatic Young's) ±Std.Deviation (MPa)	Tensile Strain (Extension) at Maximum Load ±Std. Deviation (mm/mm)	Energy at Maximum Load ± Std.Deviation (N-mm)
1.25 ± 0.26	45.71 ± 9.46	124.18 ± 38.59	1.33 ± 0.26	8.05 ± 2.07

Table 4.2: Mean and standard deviations of crimped multilayered PCL tensile testing

Figure 5.2 represents the tensile testing of crimped multilayered PCL. Table 4.2 presents the mean and standard deviations of crimped multilayered PCL tensile testing, which resulted in having a maximum load of 1.25 ± 0.26 N and a tensile stress maximum of 45.71 ± 9.46 MPa, these are the lowest numbers exhibited by any of the other PCL samples, including the single layered PCL samples and the multilayered PCL. The lower mechanical properties exhibited by crimped multilayered scaffolds are indicative that these scaffolds are weak and unlikely to be useful for the desired applications. On the other hand, crimped multilayered scaffolds exhibit the longest tensile strain (extension) at 1.33 ± 0.26 (mm/mm) from all the PCL samples, including the single layered PCL scaffolds. As a result of its low tensile stress and high extension, crimped multilayered PCL has a low Young's modulus, the lowest out of all the previously tested PCL scaffolds, at 124.18 ± 38.59 MPa. A low Young's modulus is indicative of a material that has the capacity to stretch, as is the case for the crimped multilayered scaffolds. The microhardness theory is once again in play when it comes to the crimped multilayered scaffolds and explaining why they are more flexible but weaker at the same time. When the scaffolds are multilayered, they are placed in the oven at 37°C for 15 minutes, this is their first encounter with heat. Secondly, during the crimping process they are placed in the oven, under pressure from the crimping plates at 55°C for 2 hours. The combination of heat and pressure can lead to rearrangement of the crystalline structure as has been discussed previously. The exposure to heat from the oven is also aiding in the evaporation of any excess water in the multilayered scaffolds that could still be present from the multilayering process. The evaporation of any excess water leads to a decreased ability of polar hydrogen bonding interactions between the water and the ester groups in PCL. Regular multilayered scaffolds are not subject to heating in the oven for 2 hours, it is very likely that the excess water creates hydrogen bonds with the esters and rearranges the PCL molecular structure, therefore making it stiffer and less flexible.

The multilayered PCL scaffolds are closer in range to the value reported for human ACL's as opposed to the single layered PCL scaffolds whose tensile stress values were too high. The Young's modulus for uncrimped multilayered PCL is very high and even when standard deviation is taken into account, the Young's modulus of uncrimped multilayered PCL is slightly higher than the reported human ACL Young's modulus of 111 MPa. The crimped multilayered scaffolds have a reported Young's modulus of 124.18 ± 38.59, when taking into account the standard deviations; the crimped multilayered scaffolds have a Young's modulus within the reported values of human ACL's. The single layered PCL scaffolds had reported Young's moduli that were too high in comparison to those reported for human ACL's. Both of the multilayered scaffolds have reported tensile stresses and Young's moduli that fall within the ranges of those reported for natural collagen. It can be said that overall the multilayered PCL scaffolds, specially the crimped multilayered scaffolds have mechanical properties that are closer to those of human ACL's. However, their maximum load is still too low for what is needed in a viable graft replacement requiring 1730 N for tensile stress.[15]

Figure 5.3 represents the tensile testing of multilayered PDO for 10 individual samples. Table 4.3 presents the mean and standard deviations of multilayered PDO tensile testing, which resulted in having a Young's modulus average of 520 ± 260 MPa, an average stress of 62.66 ± 35.46 MPa, and an average strain of 0.26 ± 0.11 mm/mm. Compared to previous single layer PDO scaffolds, the multilayered scaffolds have slightly higher tensile stress and maximum load. The Young's modulus for multilayered scaffolds has an enormous increase, meaning the scaffolds are extremely brittle. The tensile strain (extension) for multilayered scaffolds has decreased slightly, while the energy at maximum load remains about the same. The multilayered scaffolds are behaving as a hard and brittle material which is characterized by having a high

modulus and a low extension at failure. When we look at previous electrospun blends of PDO – beef scaffolds conducted in this lab,[59] the data shows that the beef is making the PDO scaffolds stiffer and weaker. In the case of this study, the beef gelatin seems to make the multilayered PDO scaffolds increase its Young's modulus, a sign of increased stiffness and loose extension as well.

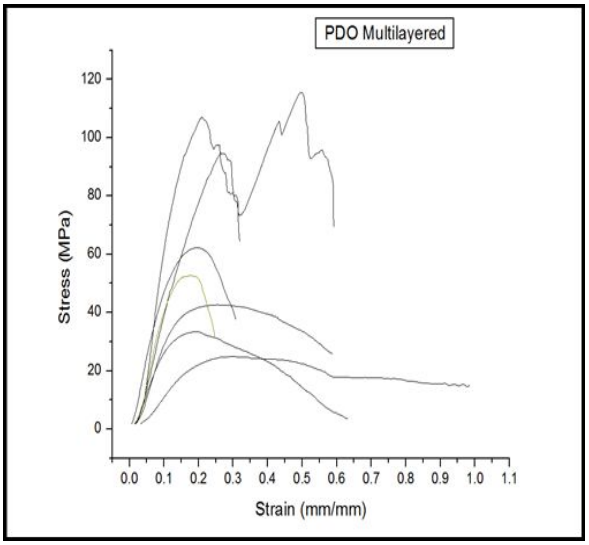

Figure 5.3: Tensile testing of individual multilayered PDO

Maximum Load ± Std. Deviation (N)	Tensile Stress at Maximum Load ±Std.Deviation (MPa)	Modulus (Automatic Young's) ±Std.Deviation (MPa)	Tensile Strain (Extension) at Maximum Load ±Std. Deviation (mm/mm)	Energy at Maximum Load ± Std.Deviation (N-mm)
1.73 ± 0.97	**62.66 ± 35.46**	**520.22 ± 260.08**	**0.26 ± 0.11**	**2.25 ± 2.27**

Table 4.3: Mean and standard deviations of multilayered PDO tensile testing

From the previous study conducted by Garcia,[59] it was indicated that the Young's modulus for PDO increased from 31.60 ± 16.00 MPa to 34.69 ± 4.72 MPa once blended with beef. There was also a decrease in extension from 2.34 ± 0.85 (mm/mm) for PDO to only 0.26 ± 0.08 (mm/mm) for the beef -PDO blends. In these two trends the PDO multilayered scaffolds match accordingly, the difference arises in the increase of tensile stress and maximum load

shown in PDO multilayered scaffolds. During the multilayering process, the PDO scaffolds are coated with the dissolved beef gelatin and are left to dry overnight, after drying overnight, the scaffolds have the look and texture similar to that of wet paper that was left to dry. They feel dry and stiff not like PCL multilayered scaffolds that still felt somewhat silky to the touch. It becomes evident even before any mechanical testing that the multilayering process has left the PDO scaffolds significantly harder and stiffer. One possible contributor to this effect could be the presence of the water and its hydrogen bonds that are interacting with the ether linkages in PDO and increasing their hydrogen bonding interactions. The increased presence of hydrogen bonds could lead to a rearrangement of the PDO molecular structure which results in brittle and hard PDO nanofibers.

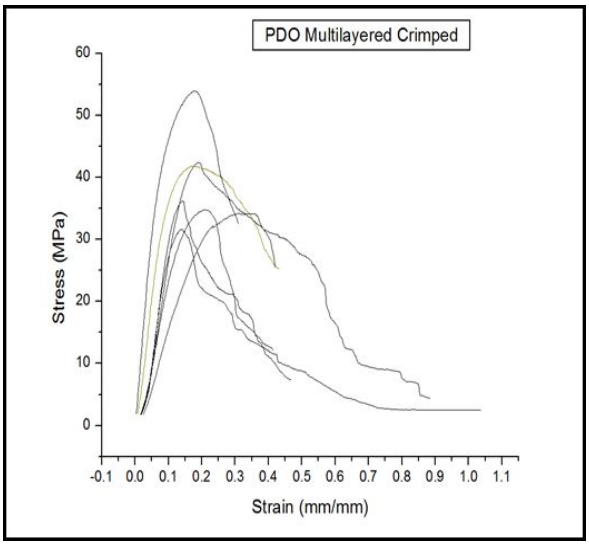

Figure 5.4: Tensile testing of individual crimped multilayered PDO

Maximum Load ± Std. Deviation (N)	Tensile Stress at Maximum Load ±Std.Deviation (MPa)	Modulus (Automatic Young's) ±Std.Deviation (MPa)	Tensile Strain (Extension) at Maximum Load ±Std. Deviation (mm/mm)	Energy at Maximum Load ± Std.Deviation (N-mm)
1.08 ± 0.20	**39.33 ± 7.56**	**418.89 ± 150.63**	**0.19 ± 0.05**	**0.94 ± 0.36**

Table 4.4: Mean and standard deviations of crimped multilayered PDO tensile testing

Figure 5.4 represents the tensile testing of crimped multilayered PDO for 10 individual samples. Table 4.4 presents the mean and standard deviations of crimped multilayered PDO tensile testing, which resulted in having a maximum load of 1.08 ± 0.20 N, a tensile stress maximum of 39.33 ± 7.56 MPa, a Young's modulus of 418 ± 150.63 MPa and an extension of only 0.19 ± 0.05 (mm/mm). The lower mechanical properties exhibited by crimped PDO multilayered scaffolds are indicative that these scaffolds are weak and can withstand only small loads. In our previous single layered PDO scaffolds the same trend occurred for crimped PDO, after the crimping process, the mechanical properties of single layered PDO seem to decrease as is the case for the crimped multilayered PDO scaffolds. However, in single layered crimped PDO scaffolds, the extension had increased significantly from 0.45 ± 0.072 (mm/mm) to 5.24 ± 0.64 (mm/mm) for the crimped PDO scaffolds. Greater extension was expected for the crimped multilayered PDO scaffolds, however the data shows that the extension decreases from 0.26 ± 0.11 (mm/mm) to the 0.19 ± 0.05 (mm/mm) for crimped multilayered PDO scaffolds. This is also the lowest extension for all PDO scaffolds done during this study. The Young's modulus of crimped multilayered PDO has decreased to 418.89 ± 150.63 MPa compared to the Young's modulus of multilayered PDO of 520.22 ± 260.08 MPa. A lowered Young's modulus is indicative of low tensile forces and higher extension rates, in the case of crimped multilayered PDO the decrease in Young's modulus is mainly driven by the fact that crimped multilayered

PDO scaffolds only withstand very low forces. As mentioned before, the properties of beef gelatin are weak and always seem to decrease the properties of the material that is combined with it, as is demonstrated by the lower mechanical properties of crimped multilayered PDO. In single layered PDO scaffolds, we observed how that is not the case for PDO samples since they actually become weaker and increase their extension. In the case of crimped multilayered PDO scaffolds, we observe the same decrease of mechanical properties but now there is also a decrease in extension. When the scaffolds are multilayered, they are placed in the oven at 37°C for 15 minutes. Secondly, during the crimping process they are placed in the oven, under pressure from the crimping plates at 85°C for 2 hours. The combination of heat and pressure can lead to rearrangement of the crystalline structure as has been discussed in the microhardness theory. In the case of multilayered PDO, there is now the added presence of water and its polar OH groups. It is evident that the water has had an effect on the crimped multilayered PDO samples since they are now the least flexible scaffolds. During the multilayering process, the hydrogen bonding interactions that occurred between the water and the ether-ester linkages in the crimped multilayered PDO scaffolds were intensified when the scaffolds were placed under pressure and heat. The placing of the crimped multilayered PDO scaffolds in the oven for 2 hours does help to evaporate some of the water present, however the hydrogen bonding interactions were already cemented in the crystalline structure of the sample. The combination of increased hydrogen bonding along with heat and pressure combining to increase the crystallinity of the ether-ester linkages of PDO, result in crimped multilayered PDO nanofibers that are weak and have lost most of their extension.

When the data is compared to the reported values for human ACL's, the multilayered PDO scaffolds have mechanical properties of much higher values. This suggests that PDO multilayered scaffolds are behaving as hard and brittle materials with un-matching characteristics of human ACL's. When we look at the reported collagen values of 5 – 500 MPa for tensile stress and 100 – 2900 MPa for Young's modulus, we see that the multilayered PDO scaffolds have mechanical properties within the ranges of collagen. What we see in the case of multilayered PDO is that the material is now behaving and exhibiting characteristics of natural collagen. It was determined to modify the multilayering method, by lowering the gelatin concentration to 0.1 % and dissolving only with hot water, in order to minimize any adverse effects of acetic acid and lower collagen levels.

Figure 5.5 illustrates the tensile testing, of 0.1% multilayered PCL for 10 individual samples. Table 4.5 presents the mean and standard deviations of multilayered PCL tensile testing, which resulted in having a Young's modulus average of 182.00 ± 96.61 MPa, an average stress of 21.54 ± 9.55 MPa, and an average strain of 0.29 ± 0.06 mm/mm.

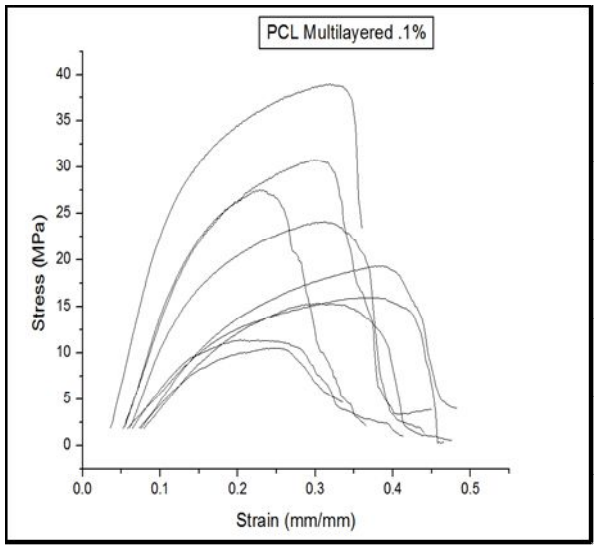

Figure 5.5: Tensile testing of individual 0.1% multilayered PCL

Maximum Load ± Std. Deviation (N)	Tensile Stress at Maximum Load ±Std.Deviation (MPa)	Modulus (Automatic Young's) ±Std.Deviation (MPa)	Tensile Strain (Extension) at Maximum Load ±Std. Deviation (mm/mm)	Energy at Maximum Load ± Std.Deviation (N-mm)
0.59 ± 0.26	21.54 ± 9.55	182.00 ± 96.61	0.29 ± 0.06	0.78 ± 0.44

Table 4.5: Mean and standard deviations of 0.1% multilayered PCL tensile testing

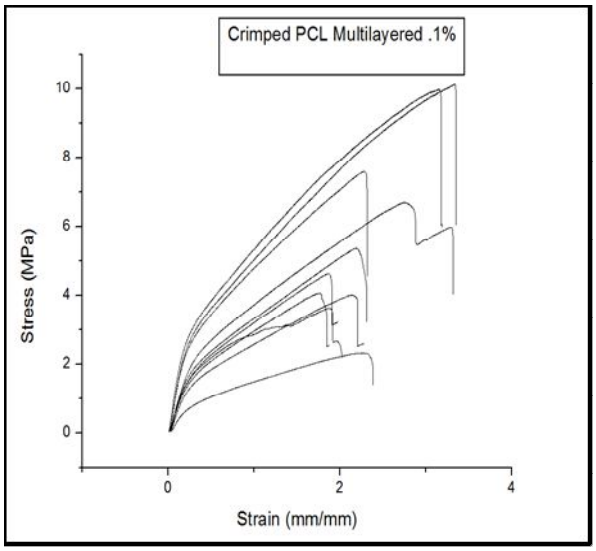

Figure 5.6: Tensile testing of individual 0.1% crimped multilayered PCL

Maximum Load ± Std. Deviation (N)	Tensile Stress at Maximum Load ±Std.Deviation (MPa)	Modulus (Automatic Young's) ±Std.Deviation (MPa)	Tensile Strain (Extension) at Maximum Load ±Std. Deviation (mm/mm)	Energy at Maximum Load ± Std.Deviation (N-mm)
6.65 ± 3.35	5.83 ± 2.68	10.45 ± 3.77	2.36 ± 0.54	83.28 ± 61.73

Table 4.6: Mean and standard deviations of 0.1% crimped multilayered PCL tensile testing

Figure 5.6 illustrates the tensile testing, of 0.1% crimped multilayered PCL for 10 individual samples. Table 4.6 presents the mean and standard deviations of crimped multilayered PCL tensile testing, which resulted in having a Young's modulus average of 10.45 ± 3.77 MPa, an average stress of 5.83 ± 2.68 MPa, and an average strain of 2.36 ± 0.54 mm/mm.

When we compare the 0.1% multilayered PCL to single layer PCL we see once again a decrease in all the mechanical properties, which we have seen is the effect the beef gelatin has on the polymer samples. In this case the concentration of beef gelatin has been decreased, therefore the effects should be less prominent. We see a decrease in Young's Modulus in the 0.1% multilayered PCL, which is now 182.00 ± 96.61 MPa, being intermediate between the Young's modulus of single layered PCL (247.23 ± 32.70 MPa) and the 1% multilayered PCL (307 ± 119 MPa). The decrease of Young's modulus in the 0.1% multilayered PCL is indicative that the 0.1% PCL is less stiff, however it does not increase the extension of the 0.1% multilayered PCL. The extension of the 0.1% multilayered PCL has dropped even further to 0.29 ± 0.06 mm/mm as opposed to 0.71 ± 0.19 mm/mm for 1% multilayered and 0.68 ± 0.055 mm/mm for single layered PCL. When we look at the 0.1% crimped multilayered, it follows the same trend as most of the crimped samples, lower mechanical properties but increased extension. For the 0.1% crimped multilayered PCL, there continues to be a decrease in Young's modulus, which is now at 10.45 ± 3.77 MPa; the flexibility of the 0.1% crimped multilayered PCL continues to increase as shown by their lower Young's modulus. The extension of the 0.1% crimped multilayered PCL has also increased to 2.36 ± 0.54 mm/mm, which is the highest extension of all the PCL samples in this study.

Figure 5.7 illustrates the tensile testing of 0.1% multilayered PDO for 10 individual samples. Table 4.7 presents the mean and standard deviations of multilayered PDO tensile testing, which resulted in having a Young's modulus average of 112.89 ± 29.05 MPa, an average stress of 15.79 ± 3.05 MPa, and an average strain of 0.98 ± 0.84 mm/mm.

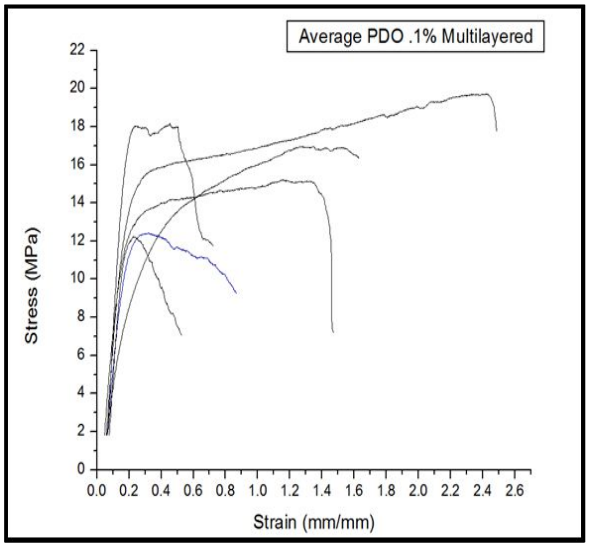

Figure 5.7: Tensile testing of individual 0.1% multilayered PDO

Maximum Load ± Std. Deviation (N)	Tensile Stress at Maximum Load ±Std.Deviation (MPa)	Modulus (Automatic Young's) ±Std.Deviation (MPa)	Tensile Strain (Extension) at Maximum Load ±Std. Deviation (mm/mm)	Energy at Maximum Load ± Std.Deviation (N-mm)
0.43 ± 0.08	**15.79 ± 3.05**	**112.89 ± 29.05**	**0.98 ± 0.84**	**2.83 ± 3.00**

Table 4.7: Mean and standard deviations of 0.1% multilayered PDO tensile testing

Figure 5.8 illustrates the tensile testing, of 0.1% crimped multilayered PDO for 10 individual samples. Table 4.8 presents the mean and standard deviations of crimped multilayered PDO tensile testing, which resulted in having a Young's modulus average of 985.62 ± 207.72 MPa, an average stress of 79.33 ± 18.54 MPa, and an average strain of 0.14 ± 0.02 mm/mm.

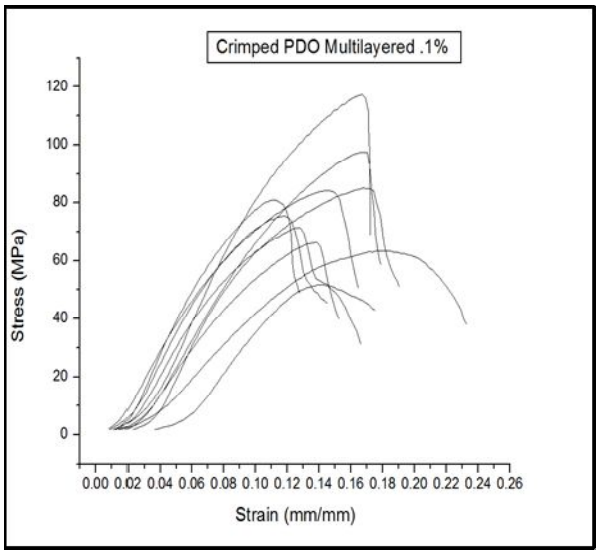

Figure 5.8: Tensile testing of individual 0.1% crimped multilayered PDO

Maximum Load ± Std. Deviation (N)	Tensile Stress at Maximum Load ±Std.Deviation (MPa)	Modulus (Automatic Young's) ±Std.Deviation (MPa)	Tensile Strain (Extension) at Maximum Load ±Std. Deviation (mm/mm)	Energy at Maximum Load ± Std.Deviation (N-mm)
2.18 ± 0.50	**79.33 ± 18.54**	**985.62 ± 207.72**	**0.14 ± 0.02**	**1.25 ± 0.45**

Table 4.8: Mean and standard deviations of 0.1% crimped multilayered PDO tensile testing

When we compare the 0.1% multilayered PDO samples to single layer PDO samples, we observe a complete set of new behavior. In the case of single layer PDO to crimped single layer PDO there was a decrease in mechanical properties but an increase in extension for crimped single layered PDO. In the 1% multilayered PDO samples, it is possible that the PDO interactions between the hydrogen bonds of water with the ether-ester groups of PDO were increasing the crystallinity of the multilayered PDO samples and decreasing their extension extensively. By decreasing the beef gelatin concentration to 0.1%, it was expected to decrease the effects of the beef gelatin and acetic acid on the polymer samples; however, the tensile

strength results of 0.1% multilayered PDO indicate different results. The 0.1% multilayered PDO samples show an increase in extension of 0.98 ± 0.84 mm/mm compared to the 0.45 ± 0.072 mm/mm of single layered PDO. The 0.1% multilayered PDO also has a decrease of Young's modulus of 112.89 ± 29.05 MPa compared to 274.73 ± 73.64 MPa for single layered PDO, indicative that the 0.1% has increased flexibility while at the same time lowered tensile stress at maximum load. In the case of single layered crimped PDO it was observed that there was a decrease in all mechanical properties, but a significant increase in extension from 0.45 ± 0.072 mm/mm to 5.24 ± 0.64 mm/mm for crimped single layered PDO. In the case of 1% multilayered PDO, it was observed that this tendency did not hold true since 1% crimped multilayered PDO decreased in all areas including extension. For 0.1% crimped multilayered PDO, we see a new trend in the results, all the mechanical properties have increased significantly and extension drops to the lowest out of all PDO samples in this study. The Young's modulus for crimped single layer PDO is 5.51 ± 3.20 MPa, for 1% crimped multilayered it is 418.89 ± 150.63 MPa and for 0.1% crimped multilayered PDO it is 985.62 ± 207.72 MPa. The extension also decreases significantly from 5.24 ± 0.64 mm/mm for crimped single layered PDO to 0.19 ± 0.05 mm/mm for 1% crimped multilayered PDO to 0.14 ± 0.02 mm/mm for 0.1% crimped multilayered PDO. From the tensile strength results for 0.1% multilayered PDO samples, it can be observed that lowering the concentration of beef gelatin did not provide the expected results. The increased concentration of water that was used in these samples could have increased the hydrogen bonding interactions between the ether –ester linkages of PDO. The combined effects of heat and pressure during the crimping process has greatly affected the 0.1% crimped multilayered PDO samples. This is observed by their significant loss of extension and their increase in Young's modulus, which is typical of hard and brittle materials.

The results obtained from multilayered tensile strength testing for both PCL and PDO and from the various concentrations proved to be irregular and inconsistent. The adverse effects of water hydrogen bonding proved to be detrimental to the extension of the polymers. It was decided that multilayering was not the adequate process to provide the characteristics that are needed for future polymer scaffold prototypes.

Twisted Tensile Testing

The third and final phase for the polymer nanofiber mats is a three strand twisted model. For this model, three 1 inch strands were cut and twisted using the custom made twisting apparatus that was built for this study. We continue to use PCL and PDO based on their exhibited mechanical properties from the single layer phase. The strands were coated with 0.1% beef gelatin only at the ends to keep them from unwinding. The ends of each strand were not used when we performed the tensile strength testing.

Figure 5.9 illustrates the tensile testing of twisted PCL for 10 individual samples. Table 4.9 presents the mean and standard deviations of twisted PCL tensile testing, which resulted in having a Young's modulus average of 16.75 ± 2.68 MPa, an average stress of 9.52 ± 0.59 MPa, and an average strain of 1.38 ± 0.24 mm/mm.

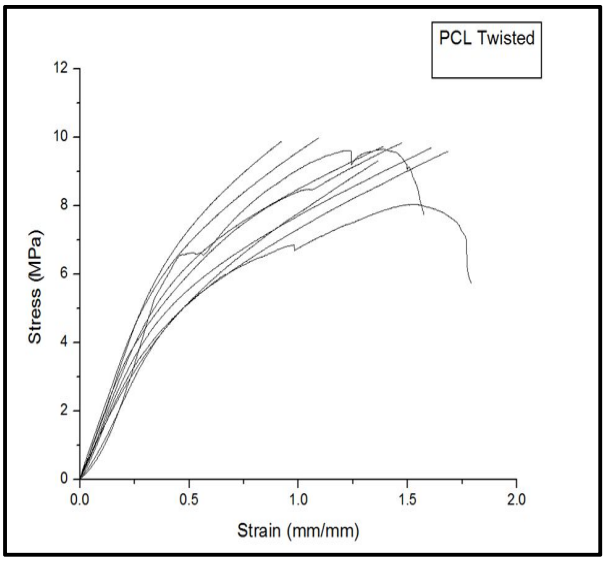

Figure 5.9: Tensile testing of individual twisted PCL

Maximum Load ± Std. Deviation (N)	Tensile Stress at Maximum Load ±Std.Deviation (MPa)	Modulus (Automatic Young's) ±Std.Deviation (MPa)	Tensile Strain (Extension) at Maximum Load ±Std. Deviation (mm/mm)	Energy at Maximum Load ± Std.Deviation (N-mm)
50.53 ± 3.95	**9.52 ± 0.59**	**16.75 ± 2.68**	**1.38 ± 0.24**	**346.26 ± 66.52**

Table 4.9: Mean and standard deviations of twisted PCL tensile testing

Figure 5.10 illustrates the tensile testing of crimped twisted PCL for 10 individual samples. Table 4.10 presents the mean and standard deviations of crimped twisted PCL tensile testing, which resulted in having a Young's modulus average of 16.60 ± 5.61 MPa, an average stress of 7.66 ± 1.39 MPa, and an average strain of 0.99 ± 0.33 mm/mm.

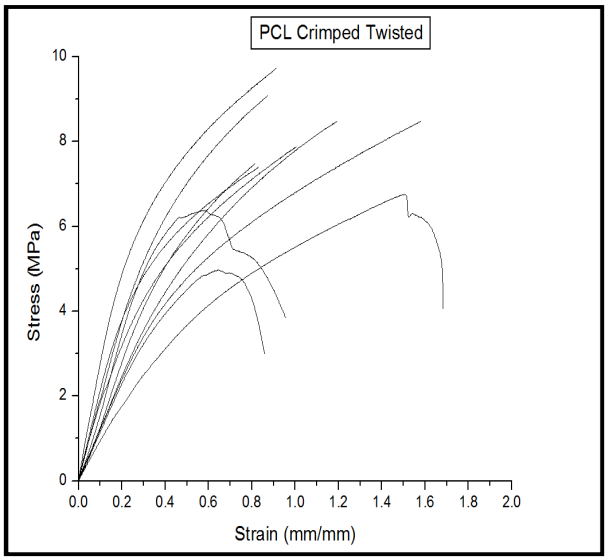

Figure 5.10: Tensile testing of individual crimped twisted PCL

Maximum Load ± Std. Deviation (N)	Tensile Stress at Maximum Load ±Std.Deviation (MPa)	Modulus (Automatic Young's) ±Std.Deviation (MPa)	Tensile Strain (Extension) at Maximum Load ±Std. Deviation (mm/mm)	Energy at Maximum Load ± Std.Deviation (N-mm)
48.96 ± 6.04	**7.66 ± 1.39**	**16.60 ± 5.61**	**0.99 ± 0.33**	**239.90 ± 89.37**

Table 4.10: Mean and standard deviations of crimped twisted PCL tensile testing

The tensile strength results for twisted PCL show some interesting tendencies. The most notable changes include the change in maximum load, for single layer PCL it is 2.27 ± 0.39 N and for 0.1% multilayered PCL it is 0.59 ± 0.26 N but for twisted PCL we see a significant increase to 50.53 ± 3.95 N. For twisted PCL we also see an increase in energy at maximum load, for single layer PCL it is 5.90 ± 1.45 N-mm, for 0.1% multilayered PCL it is 83.28 ± 61.73 and for twisted PCL it is 346.26 ± 66.52 N-mm with the possibility of this being higher since the twisted samples exceeded the limits of the tensile strength tester. For the twisted PCL, we see a decrease in tensile stress from 82.66 ± 14.38 MPa for single layer PCL, 21.54 ± 9.55 MPa for 0.1% multilayered PCL to 9.52 ± 0.59 MPa for the twisted PCL. The Young's modulus also

decreased significantly for twisted PCL to 16.75 ± 2.68 MPa compared to 247.23 ± 32.70 MPa for single layer PCL. The extension for twisted PCL also increases significantly from 0.68 ± 0.05 mm/mm for single layer PCL, 0.29 ± 0.06 for 0.1% multilayered PCL to 1.38 ± 0.24 mm/mm. For crimped twisted PCL we see the continued tendency of lowered mechanical properties for crimped samples but we do not observe an increase in extension, there is only a slight decrease in extension. For crimped twisted PCL the maximum load is still higher at 48.96 ± 6.04 N than 3.11 ± 0.71 N for crimped single layer PCL and 6.65 ± 3.35 N for crimped 0.1% multilayered PCL. The energy at maximum load is also higher for crimped twisted PCL at 239.90 ± 89.37 N-mm compared to 8.30 ± 2.95 N-mm for crimped single layer PCL and 83.28 ± 61.73 for crimped 0.1% multilayered PCL. The tensile stress for crimped twisted PCL is an intermediate value of 7.66 ± 1.39 MPa which is lower than the 113.19 ± 26.13 MPa for crimped single layer PCL but higher than the 5.83 ± 2.68 MPa for crimped 0.1% multilayered PCL. The Young's modulus for crimped twisted PCL also decreases significantly to 16.60 ± 5.61 MPa compared to 373.44 ± 80.63 MPa observed for crimped single layer PCL. This decrease in Young's modulus for both twisted PCL samples is indicative of an increase in flexibility by the twisted PCL samples. For the extension of crimped twisted PCL, we see an intermediate value of 0.99 ± 0.33 mm/mm which is higher than the single layer extension of 0.72 ± 0.12 mm/mm but lower than the crimped 0.1% multilayered PCL extension of 2.36 ± 0.54 mm/mm.

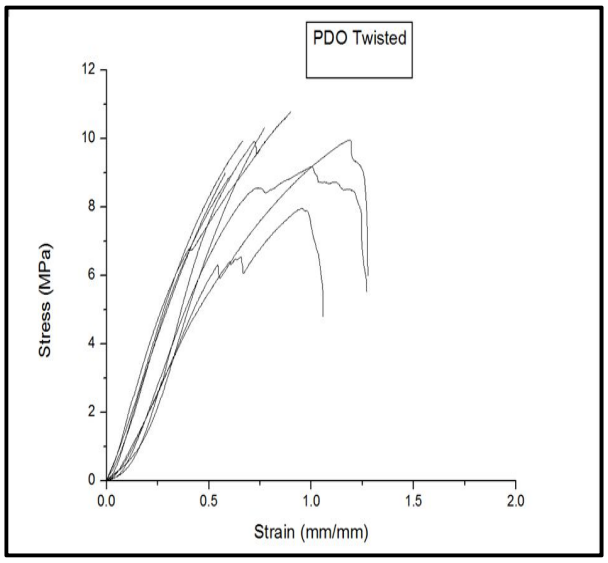

Figure 5.11: Tensile testing of individual twisted PDO

Maximum Load ± Std. Deviation (N)	Tensile Stress at Maximum Load ±Std.Deviation (MPa)	Modulus (Automatic Young's) ±Std.Deviation (MPa)	Tensile Strain (Extension) at Maximum Load ±Std. Deviation (mm/mm)	Energy at Maximum Load ± Std.Deviation (N-mm)
49.92 ± 4.98	**9.52 ± 0.85**	**18.36 ± 3.04**	**0.82 ± 0.20**	**170.16 ± 43.25**

Table 4.11: Mean and standard deviations of twisted PDO tensile testing

Figure 5.11 illustrates the tensile testing, twisted PDO for 10 individual samples. Table 4.11 presents the mean and standard deviations of twisted PDO tensile testing, which resulted in having a Young's modulus average of 18.36 ± 3.04 MPa, an average stress of 9.52 ± 0.85 MPa, and an average strain of 0.82 ± 0.20 mm/mm.

When compared to single layer PDO once again, we see an increase in maximum load for the twisted PDO samples, from 1.55 ± 0.40 N for single layer PDO, 0.43 ± 0.08 N for 0.1% multilayered PDO to 49.92 ± 4.98 N for the twisted PDO samples. There is also an increase in energy at maximum load for the twisted PDO samples, from 2.23 ± 0.75 N-mm for single layer PDO, 2.83 ± 3.00 N-mm for 0.1% multilayered PDO to 170.16 ± 43.25 N-mm for twisted PDO with the possibility of higher values since once again the twisted PDO samples exceeded the

limits of the testing equipment. The tensile stress for twisted PDO decreases to 9.52 ± 0.85 MPa compared to 56.58 ± 14.74 MPa for single layer PCL and 15.79 ± 3.05 MPa for 0.1% multilayered PDO. The Young's modulus for twisted PDO also decreases significantly to 18.36 ± 3.04 MPa compared to 274.73 ± 73.64 MPa for single layer PDO and 112.89 ± 29.05 MPa for 0.1% multilayered PDO. This decrease in Young's modulus is indicative of increase flexibility of the twisted PDO samples based on their increased extension and lowered tensile stress forces. The extension for twisted PDO samples is an intermediate value at 0.82 ± 0.20 mm/mm which is higher than 0.45 ± 0.07 mm/mm for single layer PDO but lower than 0.98 ± 0.84 for 0.1% multilayered PDO.

When we compare the tensile strength results for twisted PCL and PDO collectively and compared them to their single layer and multilayer counterparts, we observe some interesting differences in their mechanical properties. The twisted PCL and PDO prototypes exhibit outstanding values in terms of maximum load and energy absorbed at maximum load, they have the highest numbers out of all the prototypes we have conducted in this study. The future use for these polymer scaffold prototypes is to eventually be put into the human body and function as an ACL replacement and they must be able to withstand high loads. The twisted PCL and PDO prototypes have also shown that the twisting process does not affect their extension as we saw in the 0.1% multilayered prototypes that lost most of their extension. The twisting process in most cases increases the extension of PCL and PDO compared to their single layer and multilayer counterparts. The decreased tensile stress of the twisted PCL and PDO prototypes is the only mechanical property the seems to suffer greatly from the twisting process since the tensile stress for twisted PCL and PDO are the lowest out of all the PCL and PDO prototypes studied. This decrease in tensile stress is also responsible for the decreased observed in Young's modulus for

the twisted PCL and PDO prototypes. In the case of potential polymer scaffolds we do not want a scaffold that has a high value for Young's modulus since this indicated that the material is hard and brittle with little extension. We need a polymer scaffold that has a moderate Young's modulus that indicates flexibility and strength with moderate extension. The twisted PCL and PDO prototypes seem to be getting closer that intermediate value, the Young's modulus for twisted PCL and PDO is lower than for the multilayered prototypes which proved to be extremely stiff, they are also lower than the Young's modulus for single layer PCL and PDO. However, it is important to remember that the twisted PCL and PDO prototypes have decreased tensile strength and increased extensions which promote lower Young modulus values. A lowered Young's modulus does not mean that the twisted PCL and PDO prototypes are weak though since they are the strongest in terms of maximum load and energy absorbed at maximum load. The twisted prototypes show great potential in terms of finding an intermediate combination or process that will continue to optimize the mechanical properties needed for a suitable ACL replacement scaffold.

Fourier Transform Infrared Spectroscopy and Biodegradability

Figure 6.2 presents the FT - IR spectra of (a) Beef, (b) PCL, (c) PCL crimped, (d) PCL multilayered, (e) PCL crimped multilayered, (f) PCL-MMP-1and (g) PCL- Elastase. The first spectrum is of the beef gelatin powder used to make the 0.1% beef gelatin solution for the multilayered scaffolds. The beef gelatin is composed of hydroxyproline, proline, glycine and alanine as per the amino acid analysis conducted in Garcia's study.[59] The carboxylic acids are confirmed by the presence of a broad band at 3264.35 cm^{-1}, the carbonyl stretch is also

confirmed by the presence of a peak at 1626.61 cm^{-1}. The presence of N-H bending is confirmed by a moderately strong peak at 1518.66 cm^{-1}, the presence of the C-O-H bending is also confirmed by a strong peak at 1446.68 cm^{-1}. There is also evidence of C-O stretching happening at 1236.23 cm^{-1}. This spectrum will be used to identify any changes present in multilayered PCL polymer samples. The PCL spectrum (b) corresponds to single layer PCL and the carbonyl stretch is evident at 1721.01 cm^{-1} accompanied by a CH_2 bending peak at 1470.11 cm^{-1}. The C-O ester stretches correspond to moderately strong peaks displayed at 1239.85, 1162.12, 1064.89, and 1045.40 cm^{-1}. There is also a CH_2 long chain peak present at 731.51 cm^{-1}, accompanied by CH sp^3 stretches at 2940.88 and 2863.90 cm^{-1}. There are no observable peak changes for PCL crimped spectrum (c), all the observable peaks that were observed in the PCL spectrum (b) continue to be observed in the crimped PCL spectrum and confirm the PCL structure is present and has not undergone any changes. The PCL multilayered spectrum (d) contains evidence of new peaks indicating the beef gelatin has had an effect in PCL structure. In the PCL multilayered spectrum (d) the carbonyl stretch is evident at 1720.085 cm^{-1} accompanied by a CH_2 bending peak at 1470.10 cm^{-1}. The C-O ester stretches are still strong peaks displayed at 1293.83, 1239.62 and 1045.93 cm^{-1}. The CH_2 long chain peak remains present at 731.35 cm^{-1}. There are new slightly broad peaks at 1555.52 cm^{-1} and 1660.37 cm^{-1} indicative of primary amine N-H bending. There is also a slight curve at 3338.60 cm^{-1} that was not present in the single layer PCL sample and indicates –OH stretching. The PCL crimped multilayered spectrum (e) contains no observable peak differences the same peaks that were observed for PCL multilayered (d) are observed in PCL crimped multilayered (e) spectrum. The only slight difference is in the intensity of the –OH band present in PCL crimped multilayered (e) at 3324.40 cm^{-1}. The difference in intensity can be attributed to a decrease in –OH groups due to evaporation. The presence of primary amine peaks and the –OH bands present in the PCL crimped multilayered spectrum (e)

and PCL multilayered (d) help confirm our previous observations that were observed in the tensile strength testing of multilayered PCL; that the beef gelatin mixture is producing slight changes in the structure of the PCL multilayered samples. For PCL- MMP-1 spectrum (f) taken after the 4 week incubation period there are no major differences in the structure of PCL. There is only one small shoulder that appears in spectrum (f) at 1539.21cm^{-1} in the area of N-H bending. In the PCL- Elastase spectrum (g) there are also no major differences in the structure of PCL except for a very small curve appearing at 3289.73cm^{-1} in the –OH absorption region. For both spectra (f) and (g) all the conformational peaks are still present including the carbonyl peak at 1721 cm^{-1} for both. The C-O ester stretches at 1163, 1164, 1239 and 1106 cm^{-1}, the CH sp^3 stretches at 2942, 2941, 2864 and 2865cm^{-1} and the CH_2 long chain peak at 731.90 cm^{-1}. Based on the PCL spectrum after enzyme incubation, it can be said that there is not a significant amount of enzyme degradation to cause any changes to the structure of PCL.

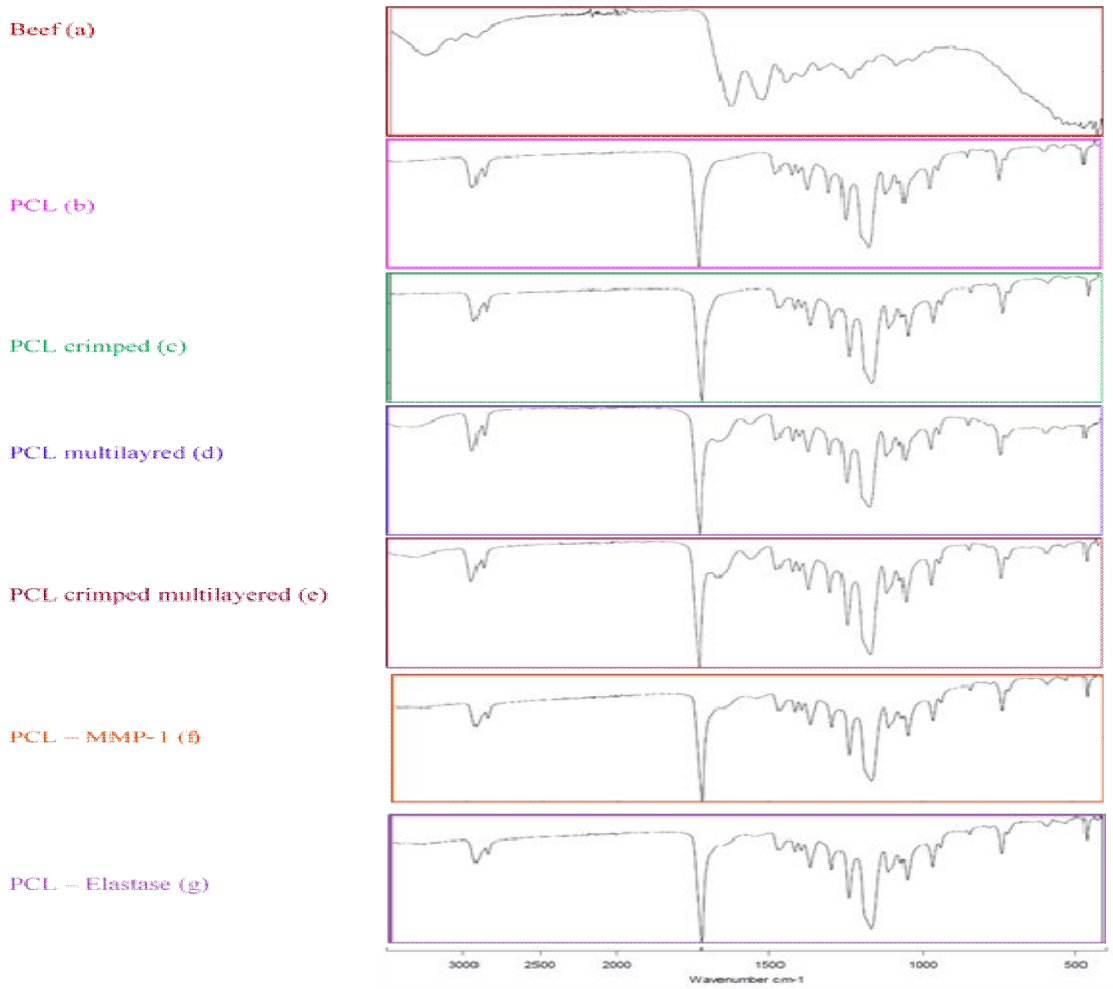

Figure 6.1: FT-IR spectra of (a) Beef, (b) PCL, (c) PCL crimped, (d) PCL multilayered, (e) PCL crimped multilayered, (f) PCL-MMP-1 and (g) PCL- Elastase.

Figure 6.2 presents the FT - IR spectra of (a) Beef, (b) PDO, (c) PDO crimped, (d) PDO multilayered, (e) PDO crimped multilayered, (f) PDO-MMP-1 and (g) PDO-Elastase. The first spectrum (a) Beef is once again of the beef gelatin powder and will be used a reference to identify any changes present in the multilayered PDO samples. The PDO spectrum (b) corresponds to single layer PDO and the carbonyl stretch is evident at 1733.37 cm^{-1}, accompanied by a CH_2 bending peak at 1453.66 cm^{-1}. The C-O ether-ester stretches are extremely strong peaks displayed at 1200.45, 1124.14 1050.12 cm^{-1}, there are also small C-H

stretches evident at 2956.88, 2924.03 and 2880.64 cm^{-1}. There are no observable peak changes for PDO crimped spectrum (c), all the observable peaks that were observed in the PDO spectrum (b) continue to be observed in the crimped PDO spectrum and confirm the PDO structure is present and has not undergone any changes. The PDO multilayered spectrum (d) contains evidence of new peaks indicating the beef gelatin has had an effect in the PDO structure. In the PDO multilayered spectrum (d) the carbonyl stretch is evident at 1733.04 cm^{-1} accompanied by a CH_2 bending peak at 1453.09 cm^{-1}. The C-O ether - ester stretches are still strong peaks displayed at 1201.29, 1125.56 and 1050.45 cm^{-1}. There are new slightly broad peaks at 1554.09 cm^{-1} and 1648.10 cm^{-1} indicative of primary amine N-H bending. The PDO crimped multilayered spectrum (e) presents even more structure changes as evident by sharp decrease in transmittance for the peaks present at 2956.47, 2915.85 2848.09 cm^{-1}. When the transmittance becomes reduced, this indicates an increase in absorptions due to more CH sp^3 molecule vibrations present in the sample. The carbonyl stretch is still present at 1732.53 cm^{-1} as well as the CH_2 bending peak at 1461.22 cm^{-1}. The C-O ether – ester stretches are strongly present as well at 1201.75, 1125.66 and1050.70 cm^{-1}. The primary N-H bending peak is still present but slightly less intense at 1652.26 and 1555.35 cm^{-1}. The presence of intense peaks in the PDO crimped multilayered spectrum (e) help confirm our previous observations that were observed in the tensile strength testing of multilayered PDO; that indeed there are water hydrogen bonding and PDO ether –ester interactions occurring, which could change the structure of the PDO multilayered samples. For PDO – MMP-1 spectrum (f) and PDO – Elastase spectrum (g) taken after the 4 week incubation period that are no observable changes from the original PDO spectrum (b). All the conformational peaks are present in the same areas including the carbonyl peak at 1732 cm^{-1} for both spectra (f) and (g), accompanied by the same strong C-O ether-ester peaks at 1126,1124, 1204, 1202 and 1050 cm^{-1}. The presence of CH sp^3 stretches is also present

at 2957, 2924 and 2919 cm^{-1} as well as the CH_2 long chain peak present at 723 cm^{-1}. The FT-IR spectra for PDO after enzyme degradation show an intact structure of PDO indicating that the PDO has not undergone any changes due to the enzymes.

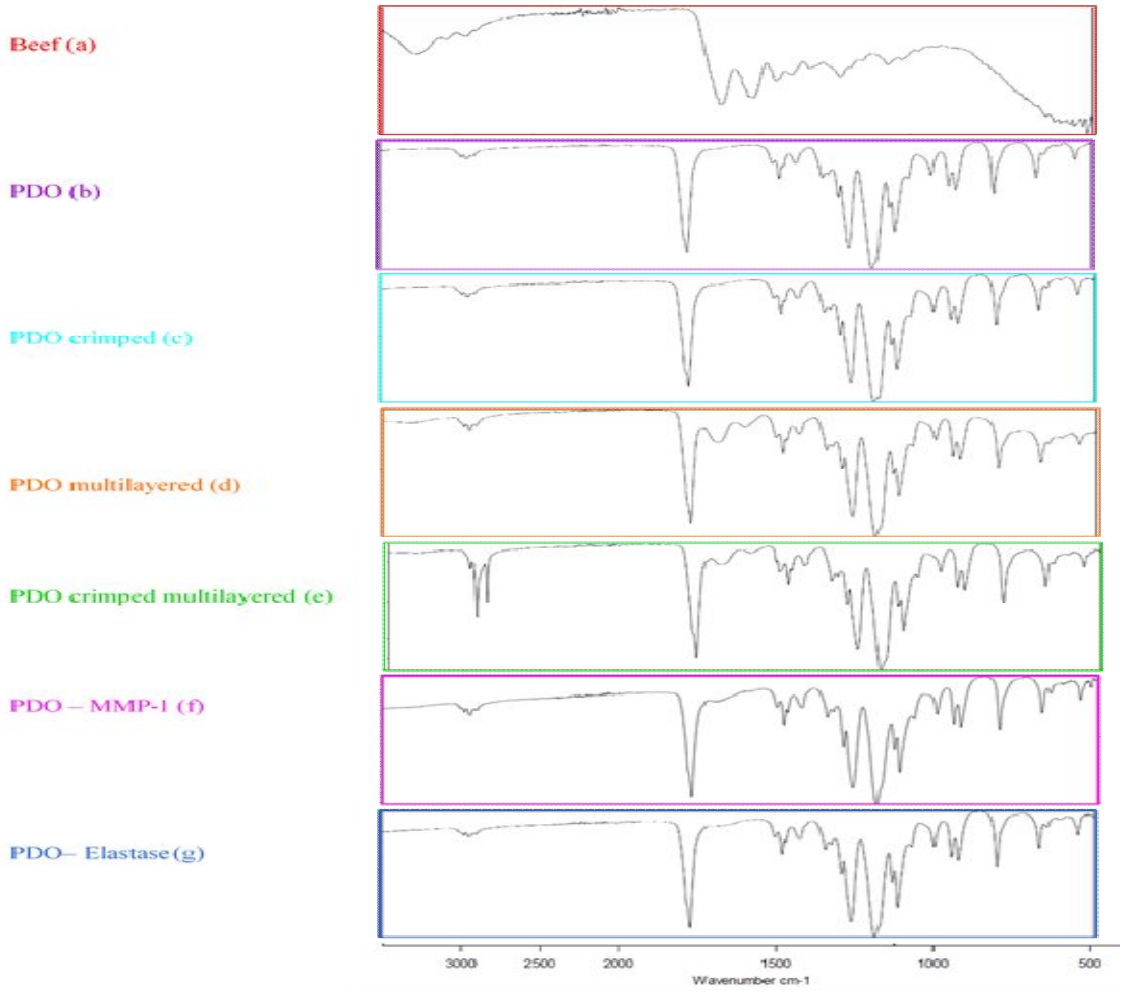

Figure 6.2: FT-IR spectra of (a) Beef, (b) PDO, (c) PDO crimped, (d) PDO multilayered, (e) PDO crimped multilayered, (f) PDO-MMP-1 and (g) PDO- Elastase.

Figure 6.3 presents the FT - IR spectra of (a) Carbothane™ 3575A, (b) Carbothane™ 3575A crimped, (c) Carbothane™ 3575A – MMP-1 and (d) Carbothane™ 3575A - Elastase. The Carbothane™ 3575A samples were not multilayered and there was no need to compare them to the previous beef spectra. In Carbothane™ 3575A spectrum (a) there can be observed a carbonyl stretch at 1736.47 cm^{-1} accompanied by CH sp^3 stretches at 2931.95 and 2858.84 cm^{-1}. The strongest peak corresponds to the C-N stretch at 1241.92 cm^{-1}, complimented by a smaller N-H out of plane peak at 952.48 cm^{-1}. CH_2 bending can be observed at 1464.23 cm^{-1} as well as N-H bending with a moderate peak at 1520.90 cm^{-1}. There is also a strong , sharp peak at 790.69 cm^{-1} that is in the area responsible for CH_2 long chain rocking .Since one of the R groups in the Carbothane™ 3575A structure is unknown this sharp peak at 790.69 cm^{-1} can be indicative of long CH_2 chains. For Carbothane™ 3575A crimped spectrum (b) there are no observable peak differences. The carbonyl peak is still observed at 1736.52 cm^{-1} as well as the strong C-N stretch at 1241.68 cm^{-1}. All the other peaks are there as well indicating the presence of CH sp^3, CH_2 bending, C-N bending, N-H out of plane as well as the CH_2 long chain peak at 790.66 cm^{-1}. The crimping process did not cause any changes to the Carbothane™ 3575A structure as shown in the FT-IR spectra. For the Carbothane™ 3575A – MMP-1 spectrum (c) and for Carbothane™ 3575A – Elastase spectrum (d) there is only one small observable difference from Carbothane™ 3575A spectrum (a). The small curve on the left side of 3000 cm-1 is now detected by the instrument and displays a signal at 3322.15 cm^{-1} for spectrum (c) and 3325.06 cm^{-1} for spectrum (d), this could indicate a slight increase in –OH or NH stretching that can occur near 3400 cm^{-1}. All the conformational peaks remain the same for spectra (c) and (d) with the carbonyl peaks present at 1735.95 and 1736.77 cm^{-1} and the extremely sharp and strong C-O, C-N stretches at 1240.83 and 1241.53 cm^{-1}. The corresponding peaks for CH sp^3, CH_2 bending, NH out of plane

and the CH_2 long chain peak at 790.63 cm^{-1} are present and confirm that the structure of Carbothane™ 3575A has not undergone any structure changes caused by the enzymes.

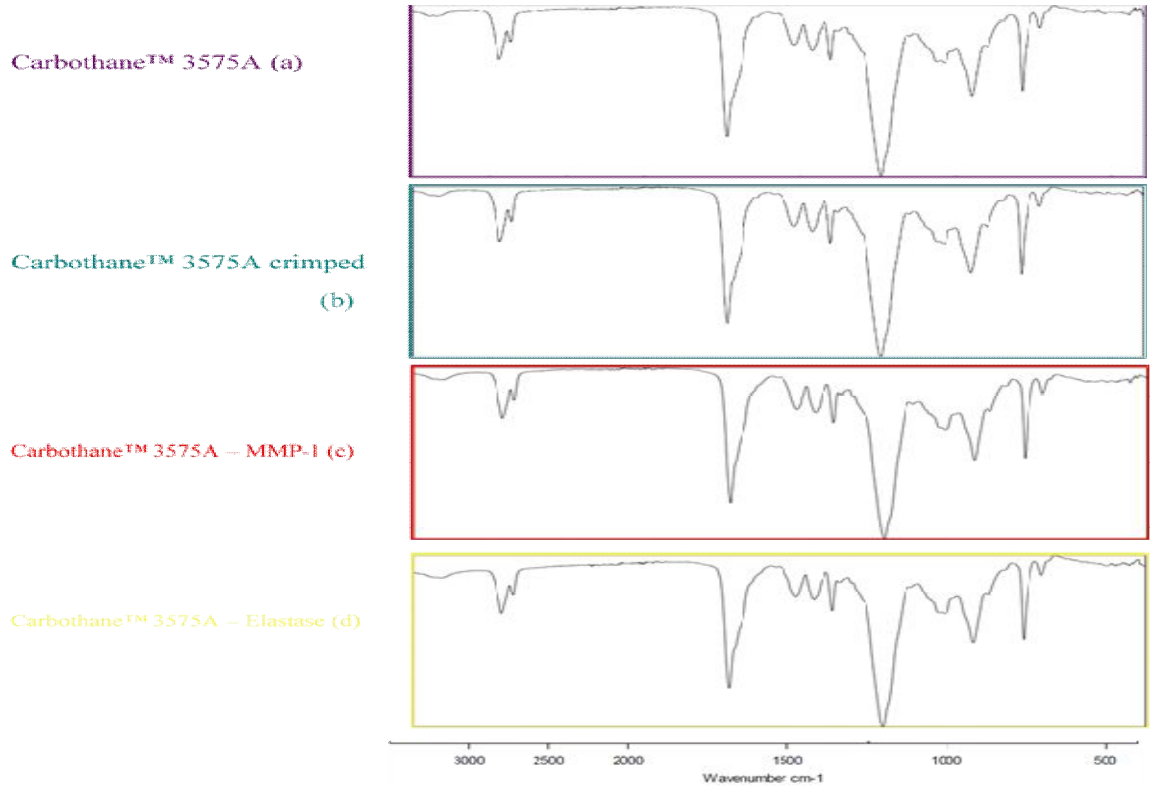

Figure 6.3: FT-IR spectra of (a) Carbothane™ 3575A, (b) Carbothane™ 3575A crimped, (c) Carbothane™ 3575A – MMP – 1 and (d) Carbothane™ 3575A – Elastase.

Figure 6.4 presents the FT - IR spectra of (a) Tecoflex™ EG 80A, (b) Tecoflex™ EG 80A crimped, (c) Tecoflex™ EG 80A- MMP-1 and (d) Tecoflex™ EG 80A – Elastase. The Tecoflex™ EG 80A samples were not multilayered and there was no need to compare them to the previous beef spectra. In Tecoflex™ EG 80A spectrum (a) there can be observed a small carbonyl stretch at 1716.45 and 1699.33 cm^{-1} accompanied by sharp CH sp^3 stretches at 2934.37 and 2852.51 and 2797.01 cm^{-1}. The strongest peak corresponds to a combination band of both C-O and C-N stretches at 1101.70 cm^{-1}. There is also a moderately strong peak at 1228.47 cm^{-1} that

is in the range for both C-O and C-N stretches. There is evidence of CH_2 bending at 1483.32 and 1447.16 cm^{-1} as well as N-H bending at 1526.17 cm^{-1}. There is a small sharp peak at 778.89 cm^{-1} corresponding to N-H out of plane bond and a small curve present at 3325.41 cm^{-1} indicative of N-H stretching that can also occur near 3400 cm^{-1}. For Tecoflex™ EG 80A crimped spectrum (b) there are no observable peak differences. The small carbonyl peak is still observed at 1716.46 cm^{-1} accompanied by the strongest peak of combined C-O and C-N stretch at 1101.44 cm^{-1}. All the other peaks are there as well indicating the presence of CH sp^3, CH_2 bending, N-H bending, N-H out of plane and the small N-H stretching curve at 3325.60 cm^{-1}. The crimping process did not cause any changes to the Tecoflex™ EG 80A structure as shown in the FT-IR spectra. For the Tecoflex™ EG 80A – MMP -1 spectrum (c) there are no observable changes with the original Tecoflex™ EG 80A spectrum (a). In the MMP-1 spectrum (c) all the conformational peaks remain the same including the small carbonyl stretch at 1715.68 and 1699cm^{-1} and the much stronger and intense C-O / C-N peak at 1101.75 cm^{-1}. The peaks for NH stretching, NH out of bond, CH_2 bending, CH sp^3 and NH bending are also present in the MMP-1 spectrum (c). Based on the FT –IR spectra of Tecoflex™ EG 80A – MMP-1 the polymer does not seem to undergo any structural changes due to this enzyme. For the Tecoflex™ EG 80A – Elastase spectrum (d) there is a significant change in structure, one of the most noticeable changes is a strong broad curve on the left side of 3000 cm-1 at 3290.42 cm^{-1}. This band has been present in previous Tecoflex™ EG 80A spectra but it had never been as intense, the increase in intensity could be due to a higher presence of CH sp^3 stretches brought about by the breaking of the $(CH_2)_4$ chain by the Elastase. There is also a significant decrease in the weak carbonyl peak, however it is still present at 1716.62 cm^{-1}. There is also a broadening of the NH and CH_2 bending peaks at 1654.82 and 1535.73 cm^{-1} respectively, indicating a higher amount of those vibrations. The C-O / C-N peak also seems to broaden and start to develop a shoulder indicating separation

of the C-O stretches at 1081.88 and C-N 1042.74 cm-1. From the Tecoflex™ EG 80A – Elastase spectrum it can be concluded that Elastase has significantly degraded the Tecoflex™ EG 80A sample. The SEM micrographs of Tecoflex EG 80A after incubation confirm this by revealing areas where the polymer has completely disappeared. This was also something that was observed visually during incubation, the Tecoflex™ EG 80A samples appeared to become paper thin and transparent indicative of drastic degradation. These effects are confirmed by FT-IR spectra, SEM and visual observations.

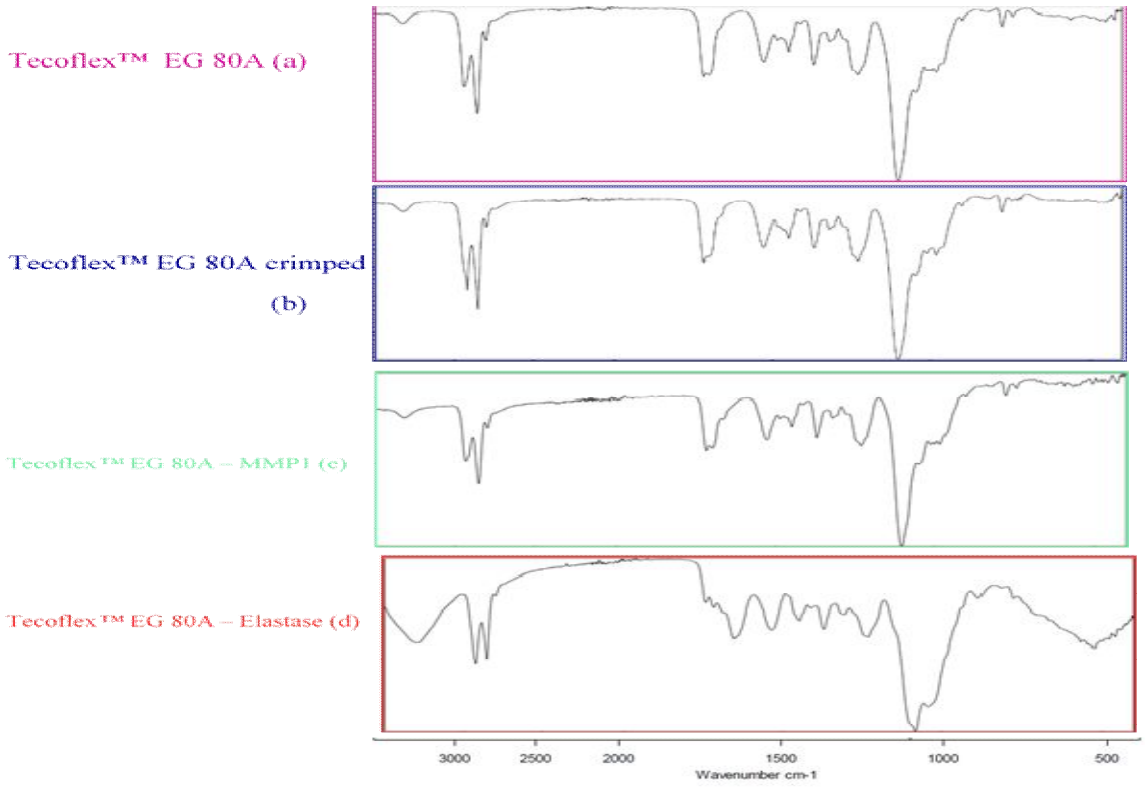

Figure 6.4: FT-IR spectra of (a) Tecoflex™ EG 80A, (b) Tecoflex™ EG 80A crimped, (c) Tecoflex™ EG 80A - MMP – 1 and (d) Tecoflex™ EG 80A – Elastase.

CHAPTER IV

CONCLUSION

When designing a scaffold for human ACL replacement, the scaffold should match the properties of younger adult ACL's in order to avoid rupture. Younger human ACL's (16 – 26 years old) are stronger and stiffer than the ACL's of older humans (48 – 86 years old). The study conducted by Noyes and Grood [50] show that younger human ACL's exhibited a tensile stress at maximum load of 37.8 ± 9.3 MPa and a Young's modulus of 111 ± 26 MPa. Of all the scaffold prototypes studied in the course of this study, there is not one that has all the definitive characteristics of a younger human ACL. The multilayered PCL scaffold at 0.1% has a tensile stress at maximum load of 21.54 ± 9.55 MPa and a Young's modulus of 182.00 ± 96.61 MPa. The values for the multilayered PCL scaffold are lower than that of the human ACL, but when the standard deviations are considered, there is an overlap of mechanical properties. However, the maximum load of the multilayered PCL scaffold was only 0.59 N, which is a very low load and not acceptable for use ACL graft replacement. The twisted PCL and PDO prototypes show increasing potential since they displayed the ability to withstand higher maximum loads of 50.53 – 48.96 ± 6.04 MPa, their tensile stress at maximum load, and Young's modulus is significantly lower than that of younger human ACL's; however, our twisted PCL and PDO prototypes could not be fully tested since they exceeded the limits of our tensile strength tester. The mechanical properties of the twisted PCL and PDO prototypes are not the accurate values and it is highly

possible that they will exhibit higher values when tested to complete failure. Another factor to consider is that the human ACL data obtained by Noyes and Grood was acquired using a strain rate of 100%/second in order to simulate fast strain rates, such as those experienced during ACL disruptions.[60] The strain rate for the scaffold prototypes done during this study was only 10 mm/min, a slow rate. Ideally these scaffolds would act as the ACL during the initial rehabilitation time for the patient, and therefore would not be subjected to high strain rates of 100%/second. Eventually, the body would be expected to start generating new ligament tissue which would have the same native properties of a healthy ACL and be able to withstand higher strain rates as the patient begins to resume normal activities.

When we look at single layer polymer scaffolds versus crimped single layer polymer scaffolds for all four polymers in this study, we see variable data. The crimping process was expected to increase the tensile stress at maximum load as well as increase the strain (extension) of the single layer polymer scaffolds. The data shows this effect is only consistent for PCL and for PDO, Tecoflex™ EG 80A and Carbothane™ 3575A, we obtain a mixture of increase only in tensile stress or an increase in extension but not both.

Multilayered PCL and PDO scaffolds show variable results as well, the multilayered scaffolds were dip coated in a 0.1% beef gelatin solution. The beef gelatin concentration was lowered throughout the study in order to minimize the effect of beef gelatin on the polymer structure. However, tensile strength testing and FT-IR testing indicate that the beef gelatin and water are having structural interactions within the polymer structure, this effect will continue to be investigated in order to fully understand how the gelatin affects the polymer scaffolds. For multilayered PCL versus crimped multilayered PCL, there is a significant decrease in tensile stress and Young's modulus, but an increase in strain and maximum load for crimped

multilayered PCL. In the multilayered PDO scaffolds there is an increase in tensile stress, Young's modulus and maximum load from uncrimped multilayered PDO to crimped multilayered PDO. Crimped multilayered PDO displays the largest decrease in extension for the multilayered scaffolds, it is believed that the crimping process along with the multilayering process has a severe effect on PDO and causes it to become hard, brittle and inflexible.

The twisted PCL and PDO scaffolds show lower tensile stress at maximum load and Young's modulus than most of the previous single layer and multilayered PCL and PDO scaffolds. There are three possible effects that could be leading to lowered mechanical properties when going from single layered scaffolds to twisted scaffolds; torsional strain effects, cross linkage decrease and the forces preventing the fibers from becoming straight.[60] However, the twisted PCL and PDO scaffolds have the greatest maximum load out of all the various scaffold prototypes tested during this study. The mechanical properties of the twisted PCL and PDO scaffolds are also inconclusive, since they exceed the limits of our tensile testing equipment. The mechanical properties for twisted PCL and PDO including tensile stress, Young's modulus and strain have the potential to be larger than what is shown in this study, and potentially get closer to the mechanical properties displayed by younger human ACL's.

The enzyme degradation studies conducted during this research serve to give us a glimpse of how our different polymer samples would be degraded by the synovial fluid enzymes, MMP-1 and Elastase. PCL shows slight degradation after four weeks, FT-IR spectra after the incubation period indicated no degradation in PCL structure. SEM fiber diameter analysis indicated a decrease in fiber diameter suggesting that the enzymes have been able to hydrolyze the carbonyl group slightly. Studies have already shown that electrospun PCL that was incubated for four weeks with rat MSCs showed mineralization and bone-specific matrix deposition within

the polymer constructs.[61] If after four weeks, PCL scaffolds are able to sustain new tissue, then the degradation shown in this study might not be an impediment and is a good indicator of a satisfactory degradation rate, while allowing for tissue formation. PDO also shows increased degradation after four weeks with increased degradations by Elastase. The FT – IR spectra indicated no degradation to the PDO structure. SEM fiber diameter analysis indicate an increase in fiber diameter after incubation with MMP-1, which could be caused by doping of MMP-1 within the fibers. Fiber diameter decreases after incubation with Elastase, indicating hydrolysis of the ether – ester bonds. Tecoflex™ EG 80A shows slight degradation by MMP-1 after four weeks, FT-IR indicates no degradation to the Tecoflex™ EG 80A structure. SEM fiber analysis indicates a decrease in fiber diameter indicating that there has been a structural change to Tecoflex™ EG 80A under MMP-1. The effect of Elastase to Tecoflex™ EG 80A was drastic, visually we could detect the Tecoflex™ EG 80A becoming paper thin during the incubation process. FT – IR indicates drastic changes in the Tecoflex™ EG 80A structure and SEM micrographs analysis show areas where the Tecoflex™ EG 80A has completely disappeared. Fiber diameter increases for Tecoflex™ EG 80A after incubation with Elastase indicating increased doping of Elastase within the fibers. Carbothane™ 3575A indicate no degradation under either enzyme, FT – IR displays no degradation to the Carbothane™ 3575A structure. Fiber diameter decreases after enzyme incubation for both enzymes indicating there has been a slight structural change to Carbothane™ 3575A. The degradation studies indicated that Carbothane™ 3575A and PCL show the least adverse effects to enzyme degradation and would be the best materials to one day potentially place inside the human knee environment.

Future work will include twisting PCL and Carbothane™ 3575A composites or blended electrospun nanofiber scaffolds of PCL and Carbothane™ 3575A. Enzyme degradation studies

will continue to be conducted with the addition of plasmin as a third enzyme. Plasmin is also found in the synovial fluid of the knee joint and it is known to degrade fibrin. Tensile strength testing along, SEM, fiber diameter analysis, and FT- IR will continue to prove invaluable to obtain the properties of the blended composites. Differential scanning calorimetry (DSC) studies will also be obtained in order to ascertain crystallinity in the polymer scaffolds.

REFERENCES

1. Vunjak-Novakovic, G., Gregory Altman, Rebecca Horan, and David L. Kaplan. "Tissue Engineering Of Ligaments." *Annual Review of Biomedical Engineering* 6.1 (2004): 131-56. Print.

2. Arnocky, S.P, Rubin, R.M, Marshall, J.L. "Microvasculature of the cruciate ligaments and its response to injury. An experimental study in dogs." 61.8 (1979):1221-1229. Web.

3. Karmani, S., and T. Ember. "The Anterior Cruciate Ligament—II." *Current Orthopaedics* 18.1 (2004): 49-57. Print.

4. Freeman, Joseph W., Mia D. Woods, and Cato T. Laurencin. "Tissue Engineering of the Anterior Cruciate Ligament Using a Braid–twist Scaffold Design." *Journal of Biomechanics* 40.9 (2007): 2029-036. Print.

5. Feagin, John A., and Walton W. Curl. "Classic Article: Isolated Tear of the Anterior Cruciate Ligament—Five-Year Follow-Up Study." *Journal of Orthopaedic & Sports Physical Therapy* 12.6 (1990): 232-36. Print.

6. Amy, E., Micheo, W., W. R. Frontera, J. K. Silver, and J. Thomas D. Rizzo, eds., "Musculoskeletal disorders: Knee and lower leg," Essentials of Physical Medicine and Rehabilitation. Musculoskeletal Disorders, Pain, and Rehabilitation. Elsevier, Philadelphia, PA, (2008) p. 307.

7. Dodds, Julie A., and Steven P. Arnoczky. "Anatomy of the Anterior Cruciate Ligament: A Blueprint for Repair and Reconstruction." *Arthroscopy: The Journal of Arthroscopic & Related Surgery* 10.2 (1994): 132-39. Print.

8. Kastelic, J., A. Galeski, and E. Baer. "The Multicomposite Structure of Tendon." *Connective Tissue Research* 6.1 (1978): 11-23. Web.

9. Anderson DD, Adams DJ, Hale JE, In Nigg, MacIntosh, Mester (Eds.). "Mechanical Effects of Forces Acting on Bone, Cartilage, Ligaments and Tendons." *Biomechanics and Biology of Movement*. Human Kinetics, Champaign, IL. (2000), (pp. 283–306).

10. Rigozzi, Samuela. *Structure and Function in Tendon: Experimental Studies on the Ultrastructural Determinants of Tendon Biomechanical Function*. Diss. Diss., Eidgenössische Technische Hochschule ETH Zürich, Nr. 19668, (2011). N.p.: n.p., n.d. Print.

11. Kastelic, J., I. Palley, and E. Baer. "A Structural Mechanical Model for Tendon Crimping." *Journal of Biomechanics* 13.10 (1980): 887-93. Print.

12. Chen, E. H., and J. Black. "Materials Design Analysis of the Prosthetic Anterior Cruciate Ligament."*Journal of Biomedical Materials Research*14.5 (1980): 567-86. Web.

13. Thomopoulos, Stavros, and Guy M. Genin. "Tendon and Ligament Biomechanics." *Orthopaedic Biomechanics*. By Beth A. Winkelstein. Boca Raton, FL: CRC, 2013. 49-74. Print.

14. Cooper, James A., Helen H. Lu, Frank K. Ko, Joseph W. Freeman, and Cato T. Laurencin. "Fiber-based Tissue-engineered Scaffold for Ligament Replacement: Design Considerations and in Vitro Evaluation." *Biomaterials* 26.13 (2005): 1523-532. Print

15 Woo SLY, Adams DJ. The tensile properties of the human anterior cruciate ligament and ACL graft tissues. In: Daniel DM, Akeson WH, O'Conner JJ, editors. Knee ligaments, structure, function, injury, and repair. New York: Raven Press; 1990. p. 279–89.

16. Altman, Gregory H., Rebecca L. Horan, Helen H. Lu, Jodie Moreau, Ivan Martin, John C. Richmond, and David L. Kaplan. "Silk Matrix for Tissue Engineered Anterior Cruciate Ligaments." *Biomaterials* 23.20 (2002): 4131-141. Print.

17. Vasita, Rajesh, and Dhirendra S. Katti. "Nanofibers and Their Applications in Tissue Engineering." *International Journal of Nanomedicine* 1.1 (2006): 15-30. Print.

18. Pelfrey, Sean, Travis Cantu, Michael R. Papantonakis, Duane L. Simonson, R. Andrew Mcgill, and Javier Macossay. "Microscopic and Spectroscopic Studies of Thermally Enhanced Electrospun PMMA Micro- and Nanofibers." *Polymer Chemistry* 1.6 (2010): 866. Print.

19. Gilbert, William. *William Gilbert of Colchester, Physician of London: On the Magnet, Magnetick Bodies.* N.p.: Chiswick for the Gilbert Club, 1900. *Gutenberg.org*. 26 Sept. 2010. Web. 13 Nov. 2014

20. Tucker, Nick, Jonathan Stanger, Mark Staiger, Hussam Razzaq, and Kathleen Hofman. "Journal of Engineered Fibers and Fabrics 63 Http://www.jeffjournal.org SPECIAL ISSUE - July 2012 – FIBERS The History of the Science and Technology of Electrospinning from 1600 to 1995." *Journal of Engineered Fibers and Fabrics* (2012): 63-73. Print

21. Bhardwaj, Nandana, and Subhas C. Kundu. "Electrospinning: A Fascinating Fiber Fabrication Technique." *Biotechnology Advances* 28.3 (2010): 325-47. Print.

22. Taylor, G. "Disintegration of Water Drops in an Electric Field." *Proceedings of the Royal Society A: Mathematical, Physical and Engineering Sciences* 280.1382 (1964): 383-97. Print.

23. Meechaisue, Chidchanok, Robert Dubin, Pitt Supaphol, Voravee P. Hoven, and Joachim Kohn. "Electrospun Mat of Tyrosine-derived Polycarbonate Fibers for Potential Use as Tissue Scaffolding Material." *Journal of Biomaterials Science, Polymer Edition* 17.9 (2006): 1039-056. Print.

24. Rim, Nae Gyune, Choongsoo S. Shin, and Heungsoo Shin. "Current Approaches to Electrospun Nanofibers for Tissue Engineering." *Biomedical Materials* 8.1 (2013): Web.

25. Teo, W. E., and S. Ramakrishna. "A Review on Electrospinning Design and Nanofibre Assemblies." *Nanotechnology* 17.14 (2006): R89-106. Print.

26. Matthews, Jamil A., Gary E. Wnek, David G. Simpson, and Gary L. Bowlin. "Electrospinning of Collagen Nanofibers." *Biomacromolecules* 3.2 (2002): 232-38. Web.

27. Woodruff, Maria Ann, and Dietmar Werner Hutmacher. "The Return of a Forgotten Polymer—Polycaprolactone in the 21st Century." *Progress in Polymer Science* 35.10 (2010): 1217-256. Print.

28. Boland, Eugene D., Branch D. Coleman, Catherine P. Barnes, David G. Simpson, Gary E. Wnek, and Gary L. Bowlin. "Electrospinning Polydioxanone for Biomedical Applications." *Acta Biomaterialia* 1.1 (2005): 115-23. Web.

29. Piskin, Erhan. "Biodegradable Polymers as Biomaterials." *Journal of Biomaterials Science, Polymer Edition* 6.9 (1995): 775-95. Web.

30. Sabino, Marcos A., Susana González, Leni Márquez, and José L. Feijoo. "Study of the Hydrolytic Degradation of Polydioxanone PPDX." *Polymer Degradation and Stability* 69.2 (2000): 209-16. Web.

31. Santerre, J.p., K. Woodhouse, G. Laroche, and R.s. Labow. "Understanding the Biodegradation of Polyurethanes: From Classical Implants to Tissue Engineering Materials." *Biomaterials* 26.35 (2005): 7457-470. Print.

32. Owen, Glasbey T., Bamford C. Henry, Al-Lamee K. Gayad, Yianni Yiannakis, and Wiles M. Charles. Graft Polymers. Biocompatibles LTD, assignee. Patent EP 0891998A1. 20 Jan. 1999. Print

33. Coe, Jerome T. *Unlikely Victory: How General Electric Succeeded in the Chemical Industry*. New York: American Institute of Chemical Engineers, 2000. Print.

34. Liao, Chia-Chun, Cheng-Chien Wang, Kuo-Chen Shih, and Chuh-Yung Chen. "Electrospinning Fabrication of Partially Crystalline Bisphenol A Polycarbonate Nanofibers: Effects on Conformation, Crystallinity, and Mechanical Properties." *European Polymer Journal* 47.5 (2011): 911-24. Web.

35. Volker Serini "Polycarbonates" in Ullmann's Encyclopedia of Industrial Chemistry, Wiley-VCH, Weinheim, 2000. Print.

36. Tang, Y.w., R.s. Labow, and J.p. Santerre. "Isolation of Methylene Dianiline and Aqueous-soluble Biodegradation Products from Polycarbonate-polyurethanes." *Biomaterials* 24.17 (2003): 2805-819. Print.

37. Finer, Y., F. Jaffer, and J.p Santerre. "Mutual Influence of Cholesterol Esterase and Pseudocholinesterase on the Biodegradation of Dental Composites." *Biomaterials* 25.10 (2004): 1787-793. Web.

38. Suyama, Tetsushi, and Yutaka Tokiwa. "Enzymatic Degradation of an Aliphatic Polycarbonate, Poly(tetramethylene Carbonate)." *Enzyme and Microbial Technology* 20.2 (1997): 122-26. Web.

39. Tang, Y. W., R. S. Labow, and J. P. Santerre. "Enzyme-induced Biodegradation of Polycarbonate Polyurethanes: Dependence on Hard-segment Concentration." *Journal of Biomedical Materials Research* 56.4 (2001): 516-28. Web.

40. Tang, Y. W., R. S. Labow, and J. P. Santerre. "Enzyme-induced Biodegradation of Polycarbonate-polyurethanes: Dependence on Hard-segment Chemistry." *Journal of Biomedical Materials Research* 57.4 (2001): 597-611. Web.

41. Msakni, Nizar, Marie-Josèphe Galmier, Marie-Joëlle Couret, Claire Szczepaniak, Bernadette Bouchon, Bertrand Souweine, and Claire Lartigue. "Complementary Mass Spectrometric Approaches and Scanning Electron Microscopy to Study the Structural Stability of Polyurethane Tunneled Dialysis Catheters after Exposure to Ethanol Solutions." *Rapid Communications in Mass Spectrometry* 27.21 (2013): 2343-354. Web.

42."Carbothane™ TPU." - *LifeScience Polymers*. N.p., n.d. Web. 04 Apr. 2014.

43.Cooper, J. A., J. S. Sahota, W. J. Gorum, J. Carter, S. B. Doty, and C. T. Laurencin. "Biomimetic Tissue-engineered Anterior Cruciate Ligament Replacement." *Proceedings of the National Academy of Sciences* 104.9 (2007): 3049-054. Print.

44. Lu, Helen H., James A. Cooper, Sharron Manuel, Joseph W. Freeman, Mohammed A. Attawia, Frank K. Ko, and Cato T. Laurencin. "Anterior Cruciate Ligament Regeneration Using Braided Biodegradable Scaffolds: In Vitro Optimization Studies." *Biomaterials* 26.23 (2005): 4805-816. Print.

45. Thomas, Vinoy, Moncy V. Jose, S. Chowdhury, Jonathan F. Sullivan, Derrick R. Dean, and Yogesh K. Vohra. "Mechano-morphological Studies of Aligned Nanofibrous Scaffolds of Polycaprolactone Fabricated by Electrospinning."*Journal of Biomaterials Science, Polymer Edition*, 17.9 (2006): 969-84. Print.

46. Palmer, Matthew, Elizabeth Stanford, and Martha M. Murray. "The Effect of Synovial Fluid Enzymes on the Biodegradability of Collage and Fibrin Clots." *National Center for Biotechnology Information*. U.S. National Library of Medicine, 20 Aug. 2011. Print.

47. Rodriguez, Ferdinand. *Principles of Polymer Systems*. Washington: Taylor & Francis, 1996. Print.

48. Odian, George G. *Principles of Polymerization*. 4th Ed. New York: McGraw-Hill, 1970. Print.

49. Noyes, FR, DL Butler, ES Grood, RF Zernicke, and MS Hefzy. "Biomechanical Analysis of Human Ligament Grafts Used in Knee-ligament Repairs and Reconstructions. *"The Journal of Bone and Joint Surgery*. 66 A.3 (1984): 344-52. Print.

50. Noyes, Frank R., and Edward S. Grood. "The Strength of the Anterior Cruciate Ligament in Humans and Rhesus Monkeys." *The Journal of Bone and Joint Surgery* A 58.8 (1976): 1074-082. Print.

51. Barnes, Catherine, Scott A.Sell, Eugene D. Boland, David G.Simpson, and Gary L. Bowlin. "Nanofiber Technology: Designing the next Generation of Tissue Engineering Scaffolds." *Advanced Drug Delivery Reviews*. 59.14 (2007): 1413-433.Print.

52. Balta Calleja, F.J. "Microhardness Relating to Crystalline Polymers." *Advances in Polymer Science* 66 (1985): 117-48. Print.

53. Sell, Scott.,Patricia S.Wolfe, Koyal Garg, Jennifer M. Mccool, Isaac A.Rodriguez, and Gary L. Bowlin. "The use of Natural Polymers in Tissue Engineering: A Focus on Electrospun Extracelluar Matrix Analogues." *Polymers*. 2.4 (2010): 522-53.Print.

54. Middleton,J. A. Tipton. "Synthetic biodegradable polymers as medical devices*". Medical plastics and Biomaterials Magazine*. (2008). Print.

55. Macossay J, Sheikh FA, Cantu T, Eubanks TM, Salinas ME, Farhangi CS, Ahmad H, Hassan MS, Khil MS, Maffi SK, Kim H, Bowling GL. "Imaging, Spectroscopic, Mechanical and Biocompatibility Studies of Electrospun Tecoflex(®) EG 80A Nanofibers and Composites Thereof Containing Multiwalled Carbon Nanotubes." *Applied Surface Science* 321 (2014): 205 – 213. Print.

56. "TECOFLEX® | Microspec Corporation | Advanced Medical Extrusions." *TECOFLEX® | Microspec Corporation | Advanced Medical Extrusions*. Web. 04 Apr. 2014.

57. Sheikh FA, Macossay J, Cantu T, Zhang X, Shamshi Hassan M, Esther Salinas M, Farhangi CS, Ahmad H, Kim H, Bowlin GL. "Imaging, spectroscopy, mechanical, alignment and biocompatibility studies of electrospun medical grade polyurethane (Carbothane™ 3575A) nanofibers and composite nanofibers containing multiwalled carbon nanotubes." *Journal of the mechanical behavior of biomedical materials* 41C (2015): 189 - 198. Print.

58. "CARBOTHANE® | Microspec Corporation | Advanced Medical Extrusions." *CARBOTHANE® | Microspec Corporation | Advanced Medical Extrusions*. Web. 04 Apr. 2014.

59. Garcia, Vanessa Lizeth. *Electrospinning Polymer Blends for Biomimetic Scaffolds for ACL Tissue Engineering*. Thesis. Thesis (M.S.)--University of Texas--Pan American, 2013. Print.

60. Walters, Valerie Irene. *Design and Analysis of a Collagenous Anterior Cruciate Ligament Replacement*. Thesis. Thesis (M.S)--Virginia Polytechnic Institute and State University, 2011. Print

61. Shin M, Yoshimoto H, Vacanti JP. "In vivo bone tissue engineering using mesenchymal stem cells on a novel electrospun nanofibrous scaffold." *Tissue Eng*. (2004): 10:33–41. Web.

BIOGRAPHICAL SKETCH

Mariana Ocampo was born in Veracruz, Mexico on January 30, 1988. At the age of 7 Mariana and her family moved to Brownsville, Texas, where she graduated from Homer Hanna High School in 2006. She was a recipient of the University Scholars Scholarship that allowed her to continue her education at the University of Texas – Pan American. In May 2010 she received her Bachelor's degree in Chemistry from the University of Texas - Pan American. On January 2012, Mariana returned to obtain her Master's degree in chemistry. Mariana worked as a graduate teaching assistant for the organic chemistry labs during the completion of her Master's degree. In 2013 Mariana joined Dr. Macossay's research team and began working on biodegradable scaffolds for ACL replacements. Mariana has also worked with Dr. Macossay in various joint projects involving the analysis of certain Kevlar fibers. On December 2014 Mariana was inducted as a member of the Golden Key National Honor Society. She obtained her Master's degree in chemistry from the University of Texas Pan – American on May 16, 2015. She plans to obtain her PhD in polymer sciences at Texas State under the Material Science, Engineering, and Commercialization program.

Permanent Mailing address: 1103 Lexington Cir. Apt B, Edinburg, Texas, 78539
Author can be reached at: mocampo22@gmail.com